

Oxygen isotope systematics of chondrule phenocrysts from the CO3.0 chondrite Yamato 81020: Evidence for two distinct oxygen isotope reservoirs

Travis J. Tenner^{a,*}, Takayuki Ushikubo^a, Erika Kurahashi^b, Noriko T. Kita^a, Hiroko Nagahara^c

^a *WiscSIMS, Department of Geoscience, University of Wisconsin-Madison, Madison, WI 53706, USA*

^b *Institut für Mineralogie, Westfälische Wilhelms-Universität Münster, Corrensstr. 24, 48149 Münster, Germany*

^c *Department of Earth and Planetary Science, The University of Tokyo, 7-3-1 Hongo, Bunkyo-ku, Tokyo 113-0033, Japan*

Received 13 February 2012; accepted in revised form 18 October 2012; Available online 29 October 2012

Abstract

High-precision oxygen three-isotope measurements of olivine and pyroxene were performed on 33 chondrules in the Yamato 81020 CO3.0 chondrite by secondary ion mass spectrometry. In chondrules where oxygen isotopes were measured in both olivine and pyroxene, the majority of grains have similar values, indicating co-magmatic crystallization. However, many chondrules contain relict grains with unique oxygen isotope ratios. A striking feature of Yamato 81020 chondrules is a bimodal distribution of oxygen isotope ratios, as those with Mg# >97 phenocrysts range in $\Delta^{17}\text{O}$ from -4.8‰ to -6.5‰ (“ -5.5‰ ” group), and those with Mg# 96–36 phenocrysts have $\Delta^{17}\text{O}$ values of -2.1‰ to -3.0‰ (“ -2.5‰ ” group). A single Mg# 99.6 barred olivine chondrule has a $\Delta^{17}\text{O}$ of -3.3‰ . We discuss that $\Delta^{17}\text{O} \sim -5.5\text{‰}$ chondrules are derivative of a reservoir with limited dust enrichment ($100\times$ Solar System), which yielded a relatively reduced chondrule-forming environment. In contrast, the $\Delta^{17}\text{O} \sim -2.5\text{‰}$ chondrules may have been influenced by ^{16}O -poor H_2O ice that sublimed and then homogenized with precursor material. The addition of H_2O , when combined with high dust enrichment ($1000\times$ Solar System) and greater bulk Fe content, could have induced an oxidized environment at high temperatures, forming Mg# 96–36 chondrules. Among the 33 chondrules studied, the Al–Mg relative ages of 20 had been obtained previously. Comparing the oxygen isotope ratios and the ^{26}Al ages of these chondrules, it is likely that the “ -5.5‰ ” and “ -2.5‰ ” oxygen isotope reservoirs existed contemporaneously. This implies that the snow line was spatially fixed during chondrule formation, and separated the CO chondrite accretion region into two distinct volumes of precursors.

© 2012 Elsevier Ltd. All rights reserved.

1. INTRODUCTION

Chondrules are a significant component of chondrites, constituting 20–80 of their volume (Scott et al., 1996). Their spheroidal shapes and igneous textures indicate formation by transient heating events early in the Solar System (Nagahara, 1981; Tsuchiyama et al., 1981; Grossman, 1988; Hew-

ins and Radomsky, 1990; Hewins, 1991, 1997; Wasson et al., 1995; Greenwood and Hess, 1996; Rubin and Krot, 1996; Yu and Hewins, 1998). In unaltered chondrites, chondrules are highly interesting because their petrologic and isotopic signatures provide many constraints on the environment from which they originated. For instance, the phase assemblage of chondrules, dominated by olivine, pyroxene, and Fe-rich metals and sulfides, indicates formation under oxidized conditions ($\log f\text{O}_2$: IW-5 to IW from 1400 to 1750 °C; Kring, 1988; Zanda et al., 1994) relative to Ca, Al-rich inclusions (CAIs, $\log f\text{O}_2 < \text{IW}-6$ from

* Corresponding author. Tel.: +1 608 262 8960; fax: +1 608 262 0693.

E-mail address: tenner@wisc.edu (T.J. Tenner).

1400 to 1750 °C; Ebel and Grossman, 2000; Grossman et al., 2008). This suggests that chondrule-forming environments were enriched in oxygen, relative to regions that produced CAIs (which are assumed to be Solar in composition; Grossman et al., 2008). Chondrules are commonly classified by the Mg# (= Mol.% MgO/[MgO + FeO]) of their constituent olivine and/or pyroxene. Type I and type II chondrules are defined as those with Mg#'s above and below 90, respectively. Based on olivine, pyroxene, and Fe-rich metal phase equilibria, type I chondrules formed at log f_{O_2} values between IW-5 and IW-2, while type II chondrules formed between IW-2 and IW (Kring, 1988).

Between chondrite groups, the proportion of type I and type II chondrules varies considerably. In carbonaceous chondrites the type I/type II ratio is about 9:1, while in ordinary chondrites the ratio is about 1:1 (Scott and Krot, 2003; Kita et al., 2010). The range of olivine Mg# in type II chondrules also differs between unaltered ordinary chondrites (Mg#_{olivine}: 70–90; Jones and Scott, 1989; Jones, 1990, 1996; Kita et al., 2010; Berlin et al., 2011) and carbonaceous chondrites (Mg#_{olivine}: 40–80; Scott and Jones, 1990; Kallemeyn et al., 1994; Kurahashi et al., 2008; Connolly and Huss, 2010; Berlin et al., 2011; Rudraswami et al., 2011; Ushikubo et al., 2012; Schrader et al., 2013). These distinctions suggest that within the accretion region of chondrites the oxygen fugacities of chondrule-forming environments (i.e. type I and type II), varied spatially, and/or evolved over time (Jones, 2012). Several factors, including the degree of dust enrichment, and variations in H₂O and/or organic concentrations in precursors could have influenced oxygen fugacity during chondrule formation (Larimer, 1975; Larimer and Bartholomay, 1979; Connolly et al., 1994; Ebel and Grossman, 2000; Fedkin and Grossman, 2006; Grossman et al., 2008; Connolly and Huss, 2010). In addition, the wide Mg# range of type II chondrules is likely compounded by variability in the bulk Fe content of their precursors.

Oxygen isotope ratios of chondrules and their internal micro-distributions are important means to trace the interaction between chondrule melt and ambient gas during heating events. Early oxygen isotope studies of unequilibrated chondrite chondrules (e.g. Clayton et al., 1983, 1984, 1991; Clayton, 1993) show significant variability in $\delta^{17}O$ and $\delta^{18}O$ (where $\delta^{17}O$ and $\delta^{18}O$ are per mil ‰ deviations from Standard Mean Ocean Water {SMOW}); Baertschi, 1976). Many chondrule data (e.g. Clayton, 1993; Krot et al., 2006a) plot on or near a slope ~ 1 line on an oxygen three-isotope diagram ($\delta^{18}O$ vs. $\delta^{17}O$), similar to the CCAM (carbonaceous chondrite anhydrous mineral) line derived from analyses of CAIs (Clayton et al., 1977). This slope ~ 1 trend is unique when compared to terrestrial materials, and its origin is likely caused by mass independent isotope fractionation from photochemical reactions of molecules in the protosolar cloud or within the protoplanetary disk (e.g. Thieme and Heidenreich, 1983; Clayton, 2002; Yurimoto and Kuramoto, 2004; Lyons and Young, 2005). Such a process led to a wide variation of observed oxygen isotope ratios in chondritic materials. For example, many CAIs are ¹⁶O-rich, with $\delta^{17}O$ and $\delta^{18}O$ values of $\sim -50\%$ (Clayton et al., 1973, 1977; Yurimoto et al.,

1998; McKeegan et al., 1998). Analyses by secondary ion mass spectrometry (SIMS) have also identified the existence of CAI-like oxygen isotope signatures from relict olivine grains in chondrules (Yurimoto and Wasson, 2002; Jones et al., 2004; Rudraswami et al., 2011; Ushikubo et al., 2012). Together, these materials have oxygen isotope ratios similar to estimates of the bulk Solar System, based on SIMS measurements of captured Solar wind ($\delta^{18}O$, $\delta^{17}O$: -59 ± 8 (2SD)‰; McKeegan et al., 2011). In contrast, products of aqueous alteration in chondrites, including carbonates (Baker et al., 2002; Benedix et al., 2003), sulfates (Airieau et al., 2005), magnetite (Rowe et al., 1994; Choi et al., 1998; Hsu et al., 2005), and secondary fayalite (Choi et al., 2000; Krot et al., 2011), are significantly ¹⁶O-poor relative to the bulk Solar System, with $\delta^{17,18}O$ values up to $+180\%$ (Sakamoto et al., 2007). In relation to the bulk Solar System and aqueous alteration phases, chondrules are intermediate in $\delta^{17}O$ and $\delta^{18}O$ (-15% to $+5\%$; Krot et al., 2006a), and so it is conceivable that their oxygen isotopic signatures were derived from the mixing of ¹⁶O-rich and ¹⁶O-poor precursors. This mixing could have started as early as 0.3 Ma after the formation of the Solar System, based on measured oxygen isotope heterogeneities in some CAIs (Yurimoto et al., 1998, 2008).

Recent advancements in multi-collector SIMS now provide for in situ oxygen three isotope ratios of chondrules at sub-‰ precision and on a micron-level scale (Kita et al., 2009, 2010). When combined with petrographic observations, high-precision SIMS allows for detailed investigations within individual chondrules. For instance, in type I chondrules from LL3 chondrites, Kita et al. (2010) found a large mass dependent isotope fractionation (5‰ range in $\delta^{18}O$) that is correlated with the bulk Mg/Si ratio of individual chondrules. This observation indicates open system oxygen isotope exchange between chondrule melt and ambient gas (e.g. Nagahara and Ozawa, 2012). Recently, Ushikubo et al. (2012) investigated chondrules in Acfer 094 (type 3.0 ungrouped carbonaceous chondrite; Grossman and Brearley, 2005) and found a bimodal distribution in oxygen isotopes, with $\Delta^{17}O$ (= $\delta^{17}O - 0.52 \times \delta^{18}O$) values of $\sim -5\%$ and $\sim -2\%$. This indicates that the parent asteroid accretion region consisted of two isotopically distinct chondrule-forming reservoirs.

The timing of chondrule formation is considered to be 1–3 million years (Ma) after CAIs, based on ²⁶Al–²⁶Mg systematics (half-life of 0.7 Ma, e.g. Kita et al., 2000; Huss et al., 2001; Mostefaoui et al., 2002; Yurimoto and Wasson, 2002; Kunihiro et al., 2004; Kurahashi et al., 2008; Hutcheon et al., 2009; Villeneuve et al., 2009; Ushikubo et al., 2010; Kita and Ushikubo, 2012). Applications of ²⁶Al chronology are made with the assumption of a homogeneous distribution of ²⁶Al in the early Solar System, which is generally accepted based on (1) similar differences of ~ 1 – 3 Ma between chondrules and CAIs, using absolute Pb–Pb age determinations (e.g. Amelin et al., 2002, 2010; Connelly et al., 2008) and (2) consistent relative ages obtained from multiple types of meteorites by using three different short-lived radioisotope chronometers, ²⁶Al–²⁶Mg, ⁵³Mn–⁵³Cr, and ¹⁸²Hf–¹⁸²W, each with different decay constants (e.g. Nyquist et al., 2009; Wadhwa et al., 2011). Kurahashi et al.

(2008) performed SIMS analyses on chondrules from the CO3.0 chondrite Yamato (Y) 81020, in order to determine their ^{26}Al – ^{26}Mg systematics, and found relative ages that overlap chondrules from LL3 chondrites (e.g. Kita et al., 2000; Mostefaoui et al., 2002), even though their oxygen isotope ratios are distinctively different; being slightly below and above the terrestrial fractionation (TF) line for CO3 and LL3, respectively (Clayton, 1993).

The chondrules investigated by Kurahashi et al. (2008) cover a wide range of Mg#’s (36–99), which implies variability in oxygen fugacity during their formation. Therefore, the focus of this study is to complement the relative ^{26}Al age data of Kurahashi et al. (2008) by performing oxygen isotope analyses on the same Y-81020 chondrules. By combining oxygen isotope ratios with the composition and relative ages of Y-81020 chondrules, our goal is to provide a comprehensive assessment of the environment from which they formed.

2. ANALYTICAL PROCEDURES

2.1. Sample selection

To attain accurate chemical and isotopic characteristics of primitive Solar System solids it is imperative that samples are pristine, emphasizing that they have minimal aqueous alteration and/or metamorphism. It has been demonstrated that Yamato 81020 is a highly unequilibrated CO chondrite, with features such as heterogeneous and Mg-rich olivine (Kojima et al., 1995; Shibata, 1996) and very fine grained, sulfur-rich and low Mg# matrix material (Kojima et al., 1995). The absence of nepheline in CAIs (Kojima et al., 1995) indicates a low degree of aqueous alteration, while an inherited equilibration temperature of >1400 °C, based on olivine–chromite thermometry (Shibata, 1996), has not been reset to lower temperatures. Using Cr distributions in FeO-rich olivine (Grossman and Brearley, 2005) and the number density of Ni-rich grains in metal (Kimura et al., 2008) Y-81020 has been classified as a petrologic 3.05 chondrite, which is suitable for study.

A total of 33 Y-81020 chondrules were investigated. Twenty have been studied previously by Kurahashi et al. (2008), who determined their relative ages, and an additional 13 were chosen based on (1) representative Y-81020 chondrule types, and (2) the ability to obtain enough SIMS analyses within a chondrule to minimize uncertainties of their oxygen isotope ratios. The chondrules investigated were from sections 56-1 and 41-1 (National Institute of Polar Research); section 41-1 was referred as “Y2” in Kurahashi et al. (2008).

2.2. Scanning electron microscopy and electron microprobe analysis

Backscattered electron (BSE) and secondary electron (SE) images of chondrules were collected with a Hitachi S-3400N scanning electron microscope (SEM) at the University of Wisconsin-Madison. An energy-dispersive X-ray spectrometer (EDS) fitted to the SEM aided in identifying chondrule phases. Suitable regions for SIMS analysis (re-

gions free of cracks/pits and foreign phases, and >15 μm in diameter) were identified from the SEM images.

Major element compositions of silicate phases were determined with a Cameca SX-51 electron microprobe (EMP) at the University of Wisconsin-Madison. Analyses were conducted with a 15 keV accelerating voltage, a 10 nA beam current, a fully focused beam for crystalline phases, and a defocused (3–10 μm) beam for mesostasis (glassy and quench textured). Peak and background counting times were 10 s each. A suite of varying endmember composition standards were used to quantify mineral phase compositions, and 4 glass standards were used to determine mesostasis compositions. Na_2O count rates were monitored on the glass standards, which had up to 9.8 wt.% Na_2O , and no appreciable count rate reduction was observed with the aforementioned beam conditions (fully focused and defocused) and analysis duration. Data reduction and corrections were performed with Probe for Windows software, which included a $\varphi(\rho Z)$ matrix correction.

2.3. SIMS oxygen three-isotope analysis

In situ oxygen three-isotope analyses of olivine and/or pyroxene in chondrules were performed in a single session with the Cameca IMS 1280 at the WiscSIMS laboratory, University of Wisconsin-Madison. Analytical conditions are similar to those reported in Kita et al. (2009, 2010). The primary Cs^+ beam was tuned to produce a 15 μm diameter spot with a primary ion intensity of 3 nA. Secondary ions of $^{16}\text{O}^-$, $^{17}\text{O}^-$, and $^{18}\text{O}^-$ were detected simultaneously using 3 Faraday cups, with count rates of approximately 2.5×10^9 , 1.0×10^6 , and 5.5×10^6 counts per second (cps), respectively. The mass resolving power (MRP at 10% height) was set to ~ 2200 for $^{16}\text{O}^-$ and $^{18}\text{O}^-$ using 2 detectors on the multi-collection array, and 4500 for $^{17}\text{O}^-$ using the axial detector (or mono-collector) at a fixed position. After each analysis $^{16}\text{OH}^-$ was monitored to determine its contribution to the $^{17}\text{O}^-$ signal according to the methods described in Heck et al. (2010). Over the course of the session the $^{16}\text{OH}^-$ contribution was negligible ($<0.1\%$) on both standards and unknowns for all but a few analyses.

To determine the external reproducibility intermittent analyses of San Carlos (S.C.) olivine ($\delta^{18}\text{O} = 5.32\%$; Kita et al., 2010) were performed as a running standard, and bracketed unknown chondrule analyses (8 measurements, 4 before and 4 after, per 11–16 unknown analyses). External reproducibility is calculated as twice the standard deviation (2SD) of brackets, and for $\delta^{18}\text{O}$, $\delta^{17}\text{O}$, and $\Delta^{17}\text{O}$ were typically 0.5‰, 0.5‰, and 0.4‰, respectively. The external reproducibility of $\delta^{18}\text{O}$ is worse than the internal uncertainty of a single analysis (typically 0.1–0.2‰), and therefore indicates a small variability in spot to spot instrumental bias (Kita et al., 2009). For this reason, the 2SD values of bracketing standard analyses represent the spot to spot reproducibility, and were assigned as the uncertainties of individual spot analyses.

In addition to spot to spot instrumental bias, it is necessary to correct for instrumental biases of unknown olivine and pyroxene analyses due to variability in endmember

compositions (EA1). This was accomplished by establishing calibrations using Fo_{100} – Fo_{60} standards for olivine, and En_{97} – En_{85} and Wo_{50} – Wo_0 for pyroxene (EA2). These standards cover the range of the majority of unknowns that were analyzed. Matrix corrections were up to 3‰, depending on the endmember composition of unknowns, and are overall greater than those reported in Kita et al. (2010). The increased matrix bias was later discovered to be caused by a relatively weak electron gun sample current setting that was used during the session. A few chondrules contain Fe-rich olivines and pyroxenes that exceed the range of standards, and therefore could have systematic errors in $\delta^{18}\text{O}$ and $\delta^{17}\text{O}$ that are greater than the instrumental bias. However, this has no effect on $\Delta^{17}\text{O}$.

For a homogeneous sample, the uncertainty of an averaged oxygen isotope ratio becomes smaller with an increasing number of spot analyses. However, as demonstrated in Kita et al. (2009), $\delta^{18}\text{O}$ values are typically limited to an accuracy of 0.3‰, even for standards with similar major element compositions. This is likely due to small differences in sample topography and/or differences in sample to sample position on the SIMS stage. As a result, a 0.3‰ uncertainty in $\delta^{18}\text{O}$ is propagated, along with the uncertainty in the average of values of multiple analyses in a given sample. For $\delta^{17}\text{O}$ a 0.15‰ uncertainty is propagated, as the SIMS instrumental bias is mass dependent ($^{18}\text{O}/^{16}\text{O}$ ratios change twice as much as $^{17}\text{O}/^{16}\text{O}$ ratios). These biases yield near-negligible uncertainties in $\Delta^{17}\text{O}$, as precision and accuracy have been demonstrated to be as low as 0.1‰ in previous studies (Goodrich et al., 2010; Heck et al., 2010; Kita et al., 2010).

After the SIMS session, SEM images were taken of the spot analyses. Twenty-two of 196 pits significantly overlapped cracks/inclusions/foreign phases (>20% of the pit) and were excluded from the dataset due to the increased likelihood for erroneous measurements.

3. PETROGRAPHY AND MINERALOGY

Petrographic and mineral descriptions of the 20 chondrules that have been previously measured for Al–Mg systematics are reported in Kurahashi et al. (2008). Descriptions of the additional 13 chondrules are reported in EA3. Chondrules are classified according to the following designations: porphyritic olivine (PO): >80% olivine; porphyritic olivine-pyroxene (POP): 20–80% olivine; and porphyritic pyroxene (PP): <20% olivine. Other chondrules include those with barred olivine textures (BO chondrules), and Al-rich chondrules, where bulk Al_2O_3 concentrations exceed 10 wt.% and show a high abundance of anorthite, high-Ca pyroxene, and Ca, Al-rich glass. Appendices EA4 and EA5 contain BSE images of all chondrules, showing SIMS pits from analyses. Selected chondrules are illustrated in Figs. 1–4. Corresponding EMP data of chondrule phases are compiled in EA6.

4. SIMS RESULTS

A total of 174 SIMS analyses of olivine, low-Ca pyroxene, and high-Ca pyroxene were used to determine the oxygen isotope ratios of Y-81020 chondrules, ranging from 1 to

10 analyses per chondrule. Twenty-three chondrules are classified as “FeO-poor” (Mg# of olivine and/or low-Ca pyroxene phenocrysts >90), and include 22 type I chondrules (16 POP, 2 PO, 3 PP, 1 BO), and 1 Al-rich chondrule. The remaining 10 are classified as “FeO-rich” (Mg# of olivine and low-Ca pyroxene phenocrysts <90), and include 8 type II PO chondrules, 1 type II PO chondrule fragment, and 1 type II BO chondrule. Oxygen three-isotope diagrams of individual chondrules are shown in Figs. 5 and 6. The majority of data plot near or on the primitive chondrule mineral (PCM) line (Ushikubo et al., 2012).

4.1. Oxygen isotope ratios of FeO-poor chondrules

In 19 of the 23 FeO-poor chondrules we obtained 3 or more SIMS spot measurements, and their data can be used to assess the degree of homogeneity of chondrule oxygen isotope ratios. Based on analytical uncertainties, and within the bounds of respective SIMS analyses, 11 FeO-poor chondrules are isotopically homogeneous (Fig. 5d–f, g, i, k, m–o, s, and t). Averaged $\Delta^{17}\text{O}$ values in 10 of the 11 chondrules range from -4.8 to -6.4 ‰. Chondrule Y01, an FeO-poor BO chondrule, is relatively ^{16}O -poor (Fig. 5t), with an averaged $\Delta^{17}\text{O}$ value of -3.3 ‰. Seven of these chondrules have analyses of coexisting olivine and low-Ca pyroxene, with or without high-Ca pyroxene (Fig. 5d, g, i, k, and m–o), and when compared, the averaged $\Delta^{17}\text{O}$ values of the phases agree to within analytical uncertainties (avg. $\Delta^{17}\text{O}_{\text{olivine}} - \text{avg. } \Delta^{17}\text{O}_{\text{pyroxene}} = +0.30 \pm 0.65$ ‰ to -0.51 ± 0.38 ‰). However, averaged pyroxene $\delta^{18}\text{O}$ values are 0.4–1.2‰ less than coexisting averaged olivine.

Nine FeO-poor chondrules with multiple analyses exhibit heterogeneous oxygen isotope ratios with data that lie along a slope-1 line (Fig. 5b, h, j, l, q, r, and u–w). However, in 7 of these chondrules multiple analyses of pyroxene produce clusters of data that are within analytical uncertainties (Fig. 5b, h, l, q, r, u, and v), and 5 have some measurements of olivine that are similar to the pyroxene clusters (Fig. 5b, l, r, u, and v). In a similar manner to the “homogeneous” FeO-poor chondrules, the pyroxene clusters are slightly, yet systematically more negative in $\delta^{18}\text{O}$ than associated olivines, by 0.1–1.4‰. If considering just the data clusters in these chondrules, the oxygen isotope ratios of Y03, Y19, Y25, Y71, and Y74 (Fig. 5b, h, l, q, and r, respectively) are similar to those of the “homogeneous” FeO-poor chondrules. Of the heterogeneous data, meaning those that do not cluster with other analyzed points within an associated chondrule, 17 are from olivine grains and 3 are from low-Ca pyroxene grains.

Chondrules Y12, Y14, and Y81 have olivine and low-Ca pyroxene phenocrysts with Mg#’s of ~ 95 , while all other FeO-poor chondrules have Mg#’s greater than 97. In each of these chondrules, we analyzed olivine and pyroxene that is ^{16}O -poor relative to most of the other FeO-poor chondrule data (Fig. 5u–w).

4.2. Oxygen isotope ratios of FeO-rich chondrules

For type II chondrules Y50, Y56, and Y59, multiple SIMS measurements yield homogeneous data on an oxygen

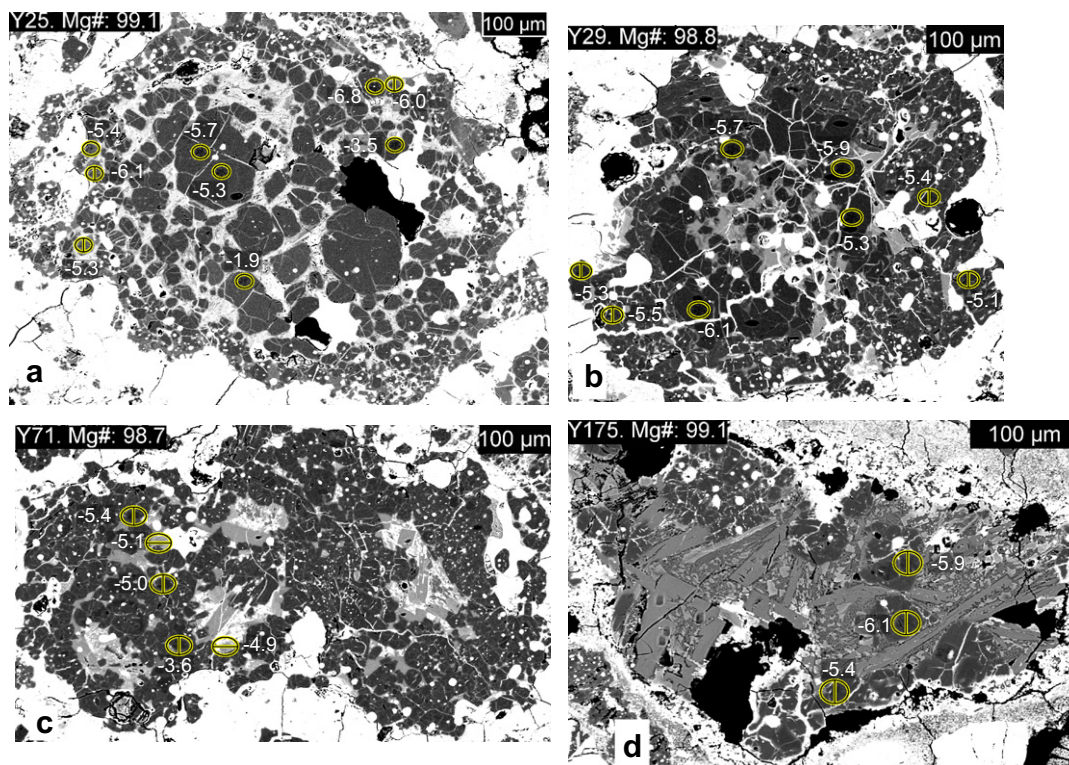


Fig. 1. BSE images of FeO-poor chondrules with Mg# >97 olivine and/or pyroxene phenocrysts. Reported chondrule Mg#'s are the average of olivine and/or low-Ca pyroxene phenocrysts. Y25, Y29, Y71, and Y175 (a–d) are POP, POP, PP, and Al-rich chondrules, respectively. Ovals denote locations of SIMS pits from oxygen isotope measurements. Open ovals correspond to olivine, and ovals with vertical and horizontal lines correspond to low-Ca pyroxene, and high-Ca pyroxene, respectively. $\Delta^{17}\text{O}$ values (‰) are shown next to each analysis. Within analytical precision chondrules Y29 and Y175 (b and d) have homogeneous oxygen isotope ratios with $\Delta^{17}\text{O}$ values of $\sim -5.5\text{‰}$. Chondrules Y25 and Y71 (a and c) have several $\Delta^{17}\text{O} \sim -5.5\text{‰}$ measurements, but also contain mineral grains that are unique in $\Delta^{17}\text{O}$.

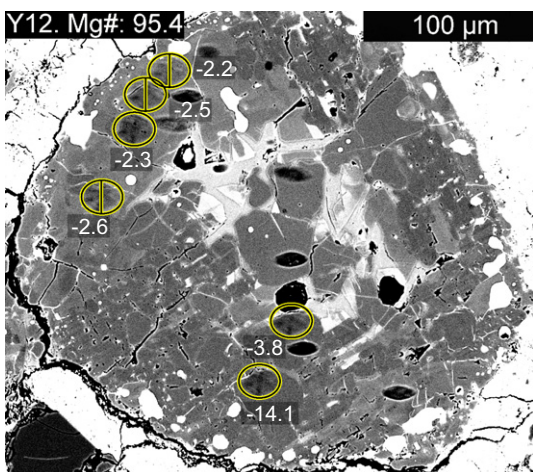


Fig. 2. BSE image of chondrule Y12, an FeO-poor, Mg# 95 POP chondrule. Chondrule Mg# is taken as average of olivine and low-Ca pyroxene phenocrysts. All symbols and terminology are the same as in Fig. 1. The olivine spot analysis in the upper left ($\Delta^{17}\text{O}$: -2.3‰) is approximately the same diameter as the olivine grain. One grain, which has a significantly different $\Delta^{17}\text{O}$ value of -14‰ , is interpreted as a relict.

three-isotope diagram (Fig. 6g, h, and j). These chondrules have nearly identical oxygen isotope ratios, as individual

spot measurements range in $\delta^{18}\text{O}$ from 0.9‰ to 2.2‰ and in $\delta^{17}\text{O}$ from -0.9‰ to -2.1‰ . Average $\Delta^{17}\text{O}$ values of Y50, Y56, and Y59 are -2.5‰ , -2.2‰ , and -2.3‰ , respectively. For each of chondrules Y2-44 and Y31 (Fig. 6c and e) we obtained only 2 spot analyses, but the data in respective chondrules are indistinguishable, and match chondrules Y50, Y56, and Y59, with averaged $\Delta^{17}\text{O}$ values of -2.4‰ and -2.1‰ , respectively. For a given chondrule the locations where SIMS analyses were performed are similar in Mg# (Figs. 3a and 6).

The remaining 5 type II chondrules, Y2-09, Y2-14, Y28, Y46, and Y58 (Fig. 6a, b, d, f, and i), exhibit heterogeneity in oxygen isotope ratios and/or the Mg# of olivine in regions where spots were analyzed. Often, the ferroan olivine grains are ^{16}O -poor when compared to coexisting olivine grains with Mg-rich cores (Figs. 3b and 6).

5. DISCUSSION

5.1. Definitions of Y-81020 host chondrule oxygen isotopic ratios and relict grains

Nearly all of the measured Y-81020 chondrules show clusters of data that are within analytical precision (Figs. 5 and 6), and in many cases these clusters consist of multiple phases (Fig. 5). If during chondrule formation, i.e. during

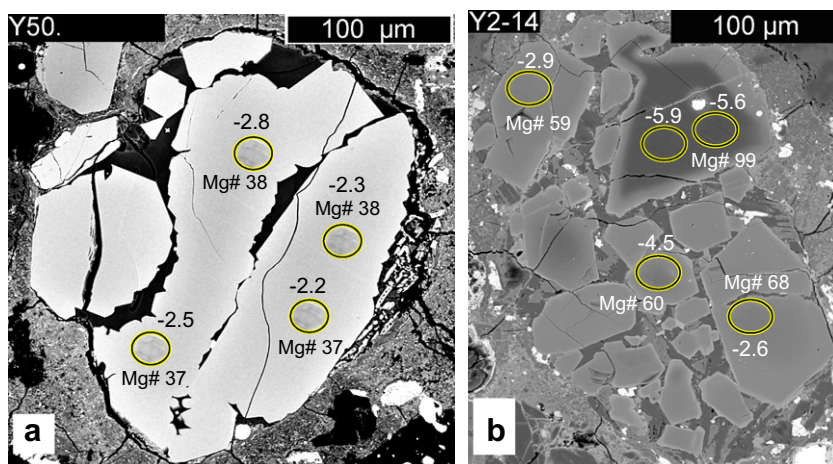


Fig. 3. BSE images of FeO-rich chondrules with Mg# <90 olivine phenocrysts. All symbols and terminology are the same as in Fig. 1. For FeO-rich chondrules in which analyzed regions of olivine have similar Mg#'s (e.g. Y50; a) their $\Delta^{17}\text{O}$ values are $\sim -2.5\text{‰}$. Several FeO-rich chondrules contain relict olivine grains with Mg-rich cores (i.e. Y2-14; b). These chondrules are typically variable in oxygen isotope ratios as well, although many ferroan grains, which presumably crystallized from the final chondrule melt, have $\Delta^{17}\text{O}$ values of $\sim -2.5\text{‰}$.

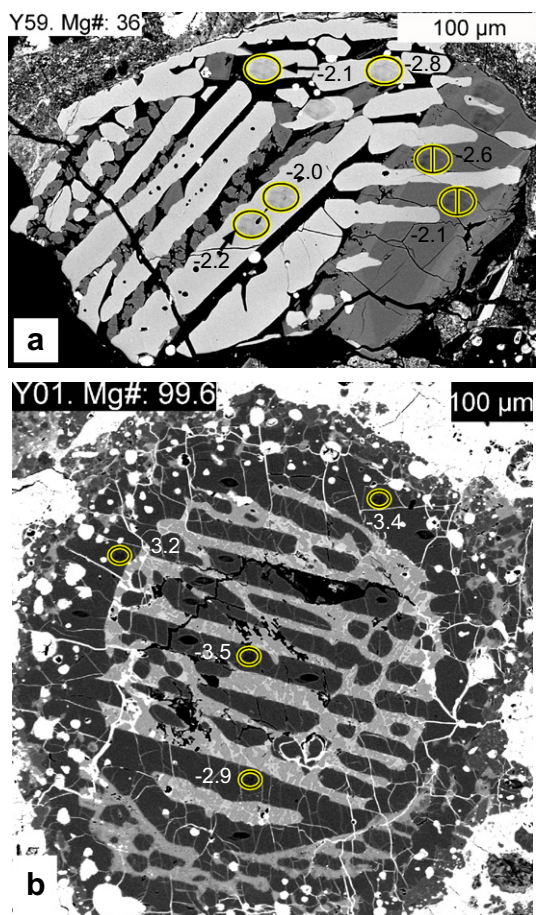


Fig. 4. BSE images of chondrules with barred olivine (BO) textures. All symbols and terminology are the same as in Fig. 1.

cooling from a molten state, the oxygen isotope composition of a chondrule remains constant, then all phases that crystallize from the melt (along with any remaining melt

that eventually forms mesostasis) should have a similar oxygen isotope composition. We define this composition as the chondrule's "host" value. It is possible, however, that the "host" oxygen isotope ratio of the chondrule melt may change over the course of cooling due to mass dependent fractionation effects between the chondrule melt and ambient gas (e.g. Kita et al., 2010; Nagahara and Ozawa, 2012), and we assess this in Section 5.2. We did not measure the oxygen isotope ratios of mesostasis because often the regions were smaller than the SIMS spot size ($\sim 15\ \mu\text{m}$) required for sub- ‰ precision analyses. It is worth mentioning, however, that measurements of glass in Acfer 094 chondrules (Ushikubo et al., 2012) are within 2‰ in $\Delta^{17}\text{O}$, when compared to coexisting olivine and pyroxene.

Many chondrules contain olivine and/or pyroxene grains with oxygen isotope ratios that are distinct relative to other coexisting measurements, and are beyond analytical uncertainties (Figs. 5 and 6). The signatures of these grains suggest that they formed from a precursor with a distinct oxygen isotope ratio, and did not equilibrate with the final chondrule melt. The oxygen isotope ratios of these "relict" grains have been preserved because oxygen diffusion rates are extremely slow in olivine (e.g. forsterite: 10^{-9} – $10^{-6}\ \mu\text{m}^2/\text{s}$ from 1100 to 1500 °C, buffered by iron-wüstite; Ryerson et al., 1989) and pyroxene (e.g. diopside: 10^{-9} – $10^{-7}\ \mu\text{m}^2/\text{s}$ from 1150 to 1300 °C, buffered by nickel-nickel oxide; Ryerson and McKeegan, 1994), meaning that diffusion distances are small over chondrule-forming durations. For example, combining the temperature dependence of the forsterite oxygen diffusion rate (i.e. Ryerson et al., 1989) with estimated chondrule cooling rates of 3×10^{-3} – $0.3\ \text{°C/s}$ (Hewins et al., 2005) yields oxygen diffusion distances of 7×10^{-4} – $7 \times 10^{-2}\ \mu\text{m}^2$ when cooling from 1500 to 1100 °C in 1 degree increments (below 1100 °C diffusion distances are less than $10^{-6}\ \mu\text{m}^2$ per 1 degree increment). The majority of measured relict grains are olivine, which could be expected because olivine is usually the highest temperature crystallizing phase in chondrules, and therefore has a high propensity to survive multiple

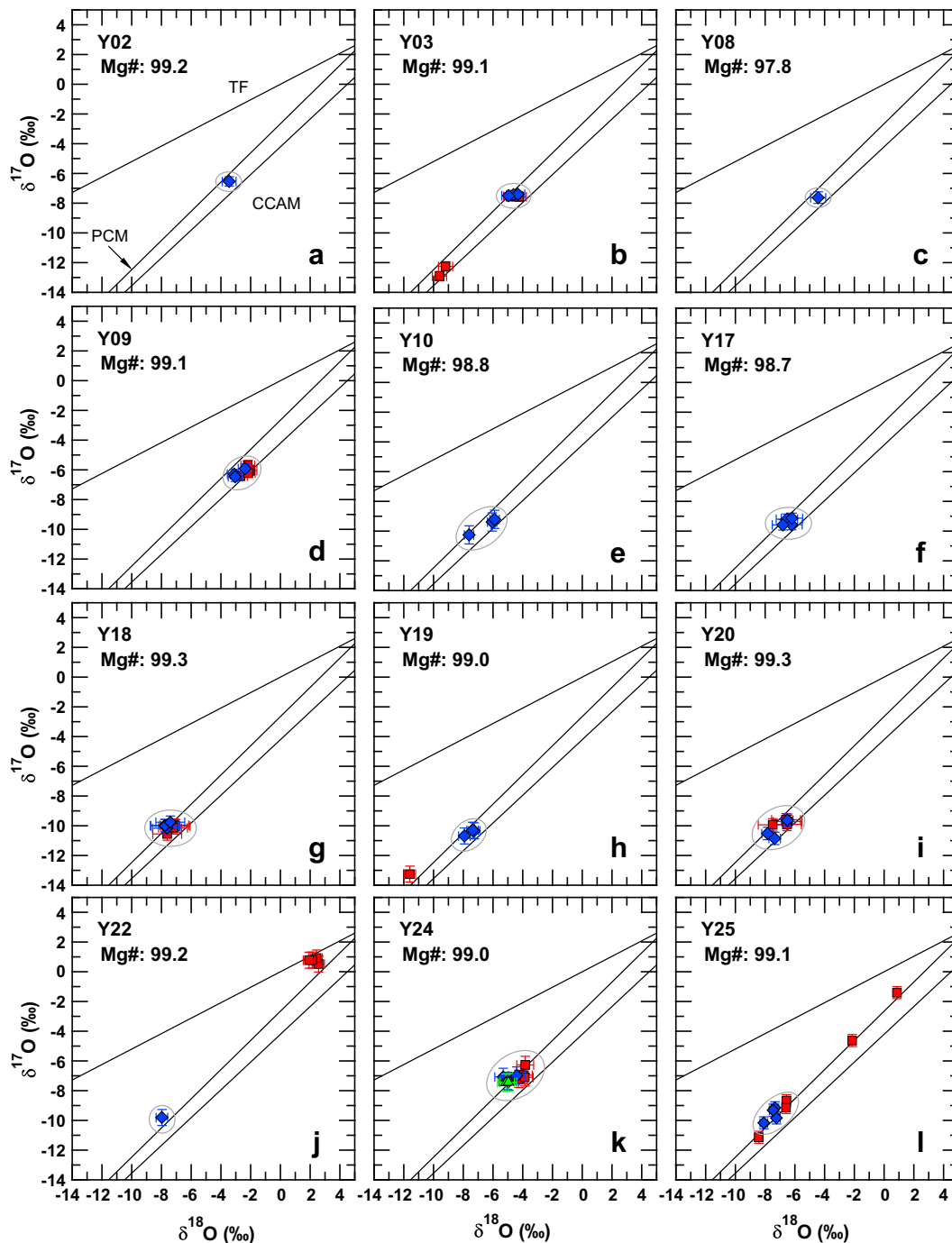


Fig. 5. Oxygen three-isotope plots of individual Y-81020 FeO-poor ($\text{Mg}\# > 90$) chondrules. Each data point represents a single SIMS spot measurement. Uncertainties are the 2SD spot to spot reproducibility, based on bracketing measurements of S.C. olivine. Reported $\text{Mg}\#$'s are the average of olivine and/or low-Ca pyroxene $\text{Mg}\#$'s within chondrules. Terrestrial fractionation (TF), carbonaceous chondrite anhydrous mineral (CCAM), and primitive chondrule mineral (PCM; Ushikubo et al., 2012) lines are shown for comparison (labeled in panel a). Data enclosed by gray ellipses are those used to determine the "host" chondrule oxygen isotope ratio. Data that are not enclosed are considered to be relict in nature. Definitions of "host" chondrule oxygen isotopic ratios and relict grains are discussed in Section 5.1.

heating events if it is close to equilibrium with the surrounding chondrule melt (Boesenberg et al., 2007). In contrast, low-Ca and high-Ca pyroxene crystallize at lower temperatures, and so their ability to survive melting events is diminished.

In addition to identification by oxygen isotope ratios, relict grains can also be defined by differences in major element chemistry, in particular $\text{Mg}\#$, relative to the other grains of the same phase within a chondrule (Nagahara, 1981; Rambaldi, 1981; Jones, 1996). This is commonly ob-

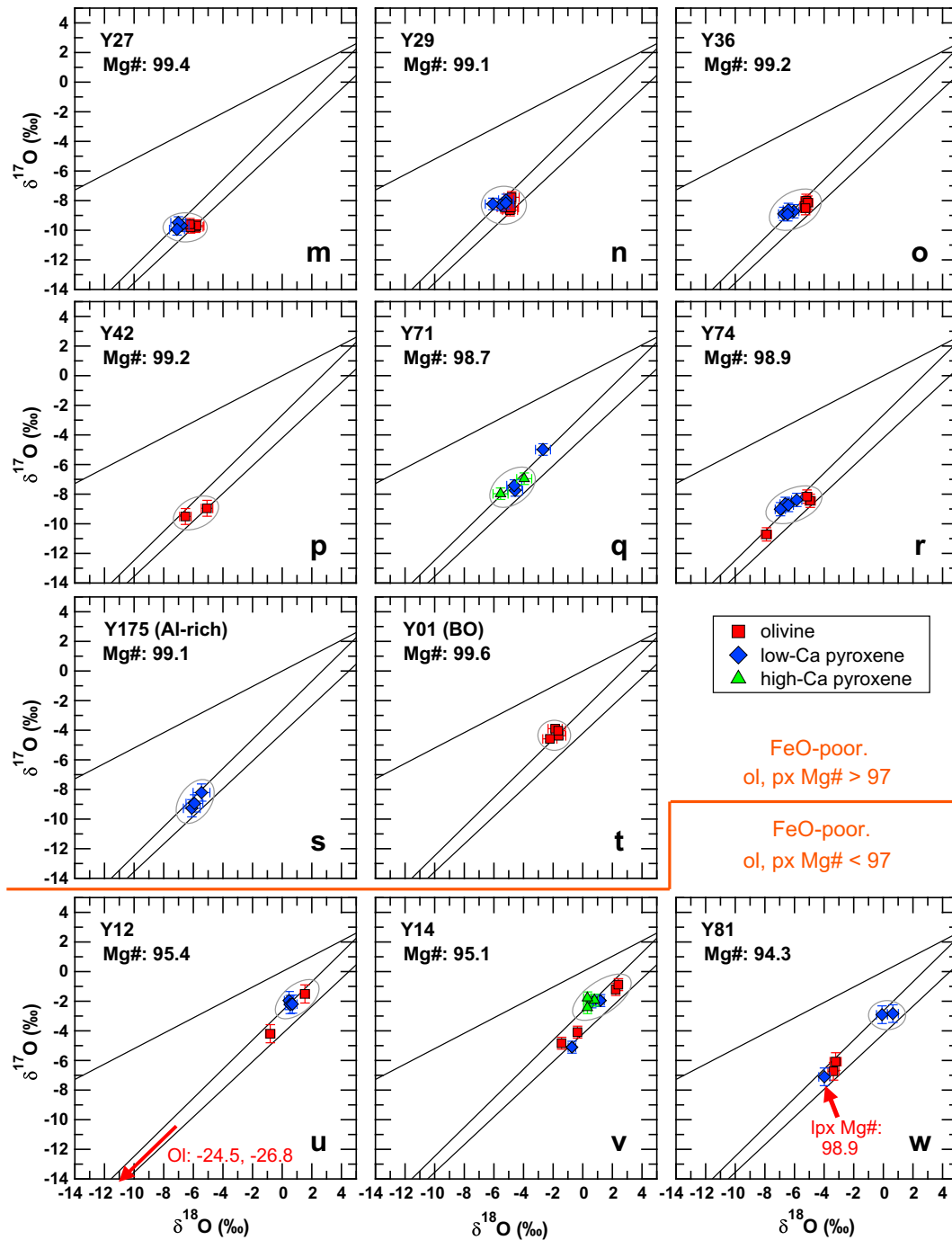


Fig. 5. (continued)

served in type II chondrules, where olivines with Mg-rich cores are often present (Jones, 1990, 1992; Johnson and Prinz, 1991; Wasson and Rubin, 2003, see also: Fig. 3b). Many of these grains have distinct oxygen isotope ratios when compared to coexisting ferroan olivine grains within the same chondrule (Jones et al., 2000, 2004; Yurimoto and Wasson, 2002; Kunihiro et al., 2004), suggesting that diffusion derived zoning of Fe and Mg, but not oxygen, is observed at the relict/overgrowth surface (Gerard and Jaoul, 1989; Cole and Chakraborty, 2001; Chakraborty,

2010). With the exception of dusty olivine grains (i.e. Nagahara, 1981) there are several cases where relict grains in FeO-poor chondrules are only identified by oxygen isotope ratios, as mineral compositions and textures are indistinguishable from other grains within the chondrule (Rudraswami et al., 2011; Ushikubo et al., 2012).

Taking into consideration the analytical uncertainties of oxygen isotope measurements and textural evidence for relict grains, we have established criteria to define SIMS spot analyses that are representative of “host” chondrule oxygen

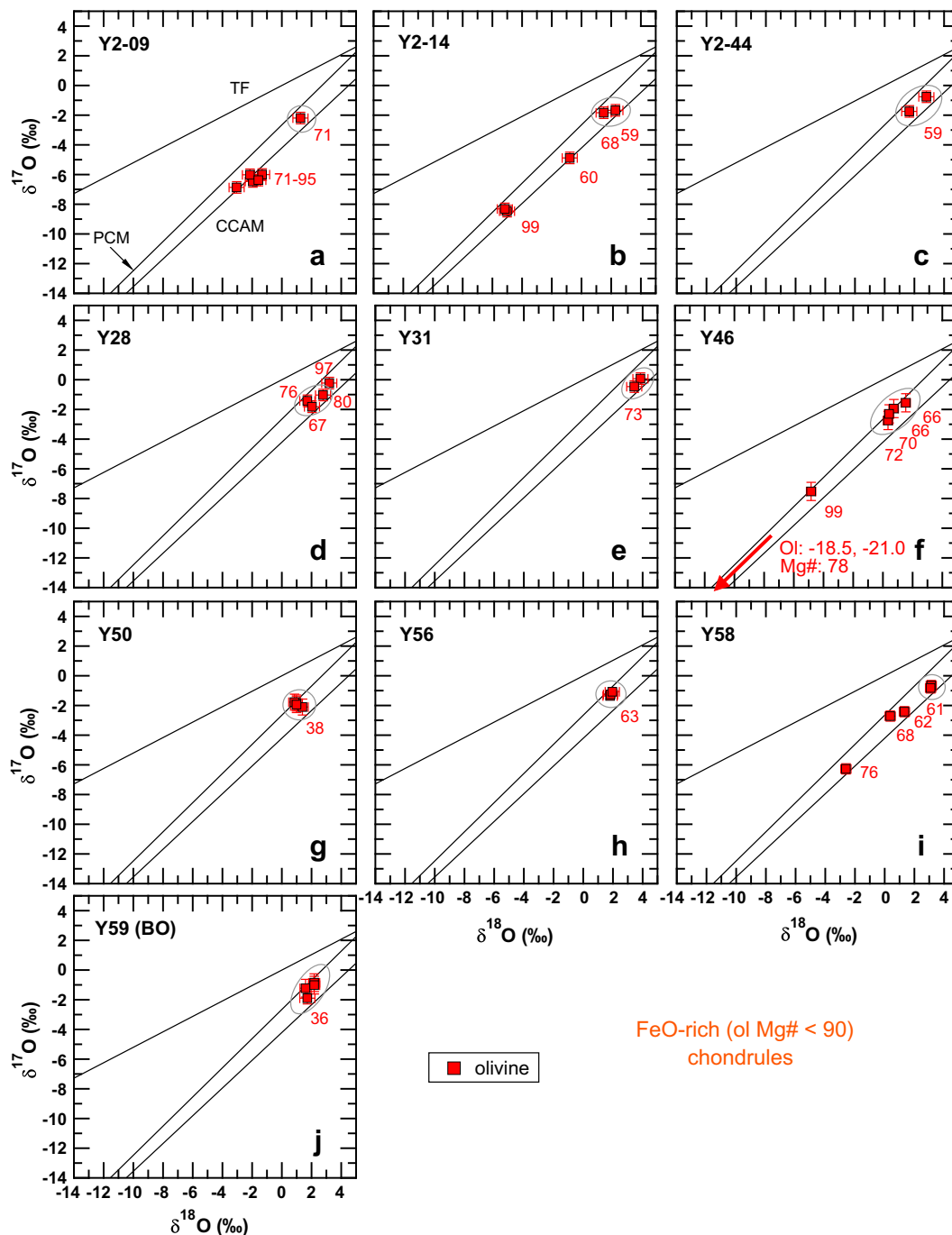


Fig. 6. Oxygen three-isotope plots of individual Y-81020 FeO-rich, type II ($Mg\# < 90$) chondrules. Each data point represents a single SIMS spot measurement. Uncertainties are the 2SD spot to spot reproducibility, based on bracketing measurements of S.C. olivine. Terrestrial fractionation (TF), carbonaceous chondrite anhydrous mineral (CCAM), and primitive chondrule mineral (PCM; Ushikubo et al., 2012) lines are shown for comparison (labeled in panel a). Numbers next to data points represent the $Mg\#$ of the region of olivine analyzed. Data enclosed by gray ellipses are those used to determine the “host” chondrule oxygen isotope ratio. Data that are not enclosed are considered to be relict in nature. Definitions of “host” chondrule oxygen isotopic ratios and relict grains are discussed in Section 5.1.

isotope ratios. This is essential in order to assess chondrule-to-chondrule relationships, and inferences regarding conditions in the early Solar System. For the analyzed Y-81020 chondrules, measurements that represent the “host” chondrule oxygen isotope ratio meet the following:

- (1) When using multiple data to determine the “host” chondrule oxygen isotope ratio, individual analyses are within the 3SD external reproducibility of $\Delta^{17}O$, relative to the average. The 3SD of $\Delta^{17}O$ is 0.6‰, based on bracketing measurements of S.C. olivine

(Section 2.3). This criterion is similar to that employed by Ushikubo et al. (2012) to determine the “host” chondrule oxygen isotope ratios in Acfer 094.

- (2) In FeO-rich chondrules with olivines that exhibit grain to grain variability in Mg#, it is assumed that analyzed grains with the lowest Mg#'s crystallized from the final chondrule-forming event (and are subsequently used for averaging, per criterion 1). Some variability in Mg# is allowed (Fig. 6b, d, and f) to account for igneous zoning, pending that oxygen isotopes of individual olivine grains meet criterion 1.
- (3) For FeO-poor chondrules, mineral grains that do not fit within criterion 1 are considered to be relict in origin. For FeO-rich chondrules, mineral grains that do not fit within criteria 1 and 2 are considered to be relict in origin.

For nearly all of the chondrules, these criteria clearly define analyses that are used to determine averaged, “host” chondrule oxygen isotope ratios, which are enclosed in gray ellipses in Figs. 5 and 6. However, some chondrules have ambiguous data, and additional considerations are applied:

- (1) For each of FeO-poor chondrules Y02 and Y08 there is only a single analysis of low-Ca pyroxene (Fig. 5a and c). We assume that these analyses represent “host” chondrule oxygen isotope ratios, but it is possible that the grains are instead relict in origin.
- (2) For FeO-poor chondrule Y22, the single low-Ca pyroxene analysis is significantly more ^{16}O -rich than measurements of coexisting olivine (Fig. 5j). We interpret that the low-Ca pyroxene analysis represents the “host” oxygen isotope ratio of the chondrule, rather than the cluster of olivine analyses. Our reasoning is twofold: (1) oxygen isotopes in pyroxene are more likely to represent that of the final chondrule melt because they likely crystallized at lower temperatures when compared to olivine; and (2) the properties of Mg-rich olivine, namely high-temperature crystallization temperatures and compositions that are in near-equilibrium with FeO-poor chondrule melts, allow for a high probability of surviving multiple chondrule heating events, while relict pyroxenes are more likely to be consumed through disequilibrium. It is possible, however, that the low-Ca pyroxene is a relict grain and that the olivine analyses represent the “host” oxygen isotope ratio of the chondrule.
- (3) For FeO-poor chondrule Y42 there are only 2 analyses of olivine, and we assume that they represent the “host” chondrule oxygen isotope ratio (Fig. 5p). The hopper textures of the olivines suggest crystallization from the final chondrule melt, but we cannot exclude the possibility that they are relict grains.
- (4) FeO-poor chondrules Y12, Y14, and Y81 contain heterogeneous data (Fig. 5u–w). However, Y14 has 3 measurements of high-Ca pyroxene with $\Delta^{17}\text{O}$ values of -2.6 , -2.3 , and -2.0 ‰ (± 0.3 ‰; EA7). As high-Ca pyroxene is one of the last phases to crystal-

ize from the melt upon chondrule cooling, we interpret these data as being representative of the “host” chondrule oxygen isotope ratio. Two additional measurements of low-Ca pyroxene, and two additional measurements of olivine have $\Delta^{17}\text{O}$ values that are within 3SD of the high-Ca pyroxene measurements (Fig. 5v; criterion 1), and they are included when determining the “host” chondrule oxygen isotope composition. Similar to chondrule Y14, chondrule Y12 has 3 measurements of low-Ca pyroxene, with $\Delta^{17}\text{O}$ values of -2.2 ‰, -2.5 ‰, and -2.5 ‰ (± 0.6 ‰; EA7). We interpret that they most likely represent the isotopic composition of the final chondrule melt. An additional olivine measurement has a $\Delta^{17}\text{O}$ value within 3SD of the pyroxene data (Fig. 5u; criterion 1), and is included when determining the “host” chondrule isotopic composition. Chondrule Y81 has two measurements of low-Ca pyroxene with $\Delta^{17}\text{O}$ values of -2.9 ‰ and -3.2 ‰ (± 0.6 ‰; EA7). The Mg# of each grain is 94.6, which is similar to other olivine and low-Ca pyroxene grains within the chondrule (EA6). We interpret that the $\Delta^{17}\text{O}$ of these measured grains are indicative of the final chondrule melt. An additional low-Ca pyroxene grain has an Mg# of 98.9 (Fig. 5w), providing petrologic evidence that it is a relict. The $\Delta^{17}\text{O}$ of this grain (-5.0 ‰) also differs from the Mg# 94.6 low-Ca pyroxenes. Collectively, these chondrules contain ^{16}O -rich relict olivine grains (Fig. 5u–w), based on these interpretations.

- (5) FeO-rich chondrule Y2-09 is dominated by olivine grains with Mg-rich cores (EA5), providing textural evidence that they are relicts. 5 spot analyses of olivine grains with cores ranging in Mg# from 71 to 95 are ^{16}O -rich ($\Delta^{17}\text{O}$ values ranging from -4.9 to -5.5 ‰), when compared to a single spot analysis of a homogeneous Mg# 71 olivine grain, which has a $\Delta^{17}\text{O}$ of -2.8 ‰ (Fig. 6a). Therefore, we interpret that the -2.8 ‰ grain crystallized from the final chondrule melting event, and represents the “host” chondrule oxygen isotope ratio.
- (6) FeO-rich chondrule Y28 contains an olivine grain with an Mg# 96.5 core (EA5). Although the $\Delta^{17}\text{O}$ of this grain (-1.9 ‰) is similar to others (-2.6 ± 0.3 ‰), its texture indicates that it is a relict.

Averaged “host” oxygen isotope ratios of Y-81020 chondrules are given in Table 1. Oxygen isotope ratios of relict grains are shown in Table 2. EA7 summarizes individual spot analyses.

5.2. The relationship between co-magmatic olivine and pyroxene during FeO-poor chondrule formation

Few data exist that provide oxygen isotope comparisons of coexisting phases within chondrules from unaltered (≤ 3.2) chondrites. An intra-phase comparison is highly valuable because it allows for an assessment of mass dependent fractionation that may have occurred during chondrule formation due to open-system effects. In this study,

Table 1
 "Host" oxygen isotope ratios (‰), Mg#^as, and relative ages of Yamato 81020 chondrules.

Chondrule	Texture	<i>n</i> (ol, lpx, hpx)	$\delta^{18}\text{O}$	Unc.	$\delta^{17}\text{O}$	Unc.	$\Delta^{17}\text{O}$	2SE	$\Delta^{17}\text{O}2\text{SD}$	Mg# ^a	Rel. age to CAI (Ma) ^b
<i>Type I. Mg# >97</i>											
Y02	POP	0,1,0	-3.5	0.6	-6.5	0.3	-4.8	0.2	n.a.	99.2	2.51(-0.79/+inf)
Y03	POP	2,3,0	-4.6	0.4	-7.5	0.2	-5.1	0.2	0.3	99.1	1.81(-0.29/+0.40)
Y08	PP	0,1,0	-4.4	0.6	-7.6	0.5	-5.3	0.4	n.a.	97.8	2.01(-0.26/+0.35)
Y09	POP	4,3,0	-2.5	0.4	-6.1	0.3	-4.8	0.2	0.4	99.1	2.09(-0.27/+0.36)
Y10	POP	0,3,0	-6.5	1.1	-9.6	0.7	-6.2	0.3	0.2	98.8	1.66(-0.25/+0.33)
Y17	POP	0,4,0	-6.4	0.5	-9.4	0.3	-6.0	0.2	0.5	98.7	2.14(-0.45/+0.80)
Y18	POP	4,4,0	-7.5	0.5	-10.1	0.2	-6.2	0.2	0.5	99.3	2.20(-0.28/+0.39)
Y19	PP	0,3,0	-7.5	0.5	-10.4	0.3	-6.5	0.3	0.1	99.0	
Y20	POP	4,3,0	-7.0	0.5	-10.0	0.4	-6.4	0.2	0.6	99.3	1.83(-0.51/+1.01)
Y22	POP	0,1,0	-8.0	0.5	-9.8	0.6	-5.7	0.5	n.a.	99.2	
Y24	POP	4,4,2	-4.6	0.5	-7.1	0.3	-4.8	0.2	0.5	99.0	1.94(-0.15/+0.17)
Y25	PO	2,4,0	-7.2	0.6	-9.4	0.5	-5.6	0.3	0.7	99.1	
Y27	POP	4,3,0	-6.4	0.5	-9.7	0.2	-6.4	0.2	0.6	99.4	
Y29	POP	4,4,0	-5.2	0.4	-8.3	0.3	-5.5	0.3	0.7	98.8	2.13(-0.18/+0.21)
Y36	POP	4,4,0	-5.8	0.6	-8.5	0.3	-5.5	0.2	0.3	99.2	
Y42	PO	2,0,0	-5.8	1.5	-9.2	0.6	-6.2	0.3	0.3	99.2	
Y71	PP	0,2,2	-4.7	0.7	-7.5	0.5	-5.2	0.2	0.4	98.7	2.29 (-0.25/+0.32)
Y74	POP	2,4,0	-6.0	0.7	-8.6	0.3	-5.5	0.2	0.5	99.0	
<i>Al-Rich</i>											
Y175	px rich	0,3,0	-5.8	0.5	-8.8	0.6	-5.8	0.4	0.7	99.1	1.91(-0.14/+0.17)
<i>Type I. Mg# <97</i>											
Y12	POP	1,3,0	0.8	0.6	-2.0	0.4	-2.4	0.3	0.3	95.4	2.14(-0.27/+0.36)
Y14	POP	2,2,3	1.1	0.7	-1.8	0.4	-2.3	0.2	0.5	95.1	
Y81	POP	0,2,0	0.3	0.8	-2.9	0.4	-3.0	0.4	0.4	94.3	
<i>Type II</i>											
Y2-09	PO	1,0,0	1.3	0.6	-2.2	0.4	-2.9	0.4	n.a.	71.0	2.03(-0.15/+0.17)
Y2-14	PO	2,0,0	1.9	0.9	-1.8	0.3	-2.7	0.3	0.3	59,68	2.01(-0.47/+0.88)
Y2-44	frag.	0,2,0	2.2	1.2	-1.3	1.0	-2.4	0.4	0.6	58.9	2.99(-0.29/+0.41)
Y28	PO	3,0,0	2.2	0.7	-1.4	0.5	-2.6	0.3	0.6	66–80	
Y31	PO	2,0,0	3.6	0.5	-0.2	0.6	-2.1	0.3	0.4	72.5	
Y46	PO	4,0,0	0.8	0.6	-2.1	0.5	-2.5	0.3	0.6	66–72	2.50(-0.35/+0.52)
Y50 ^c	PO	4,0,0	1.1	0.4	-1.9	0.3	-2.5	0.3	0.5	38	
Y56	PO	3,0,0	1.9	0.4	-1.2	0.2	-2.2	0.2	0.2	63.3	2.22(-0.23/+0.30)
Y58	PO	2,0,0	3.1	0.6	-0.7	0.3	-2.4	0.2	0.2	60–62	2.29(-0.43/+0.75)
<i>BO</i>											
Y01	FeO-poor	4,0,0	-1.8	0.4	-4.2	0.4	-3.3	0.3	0.5	99.6	2.46 (-0.27/+0.36)
Y59 ^c	FeO-rich	4,2,0	1.9	0.4	-1.3	0.5	-2.3	0.3	0.7	35.8	

$\delta^{18}\text{O}$, $\delta^{17}\text{O}$ propagated uncertainties combine a 0.3, 0.15‰ analytical uncertainty (Section 2.3) with the maximum of either the spot measurements or bracketing 2SD. The $\Delta^{17}\text{O}$ 2SE uses the maximum of either the 2SD of measurements or the bracketing 2SD.

^a Mg# is taken as the average of olivine and/or low-Ca pyroxene analyzed by EMP (EA6).

^b Relative ages are taken from Kurahashi et al. (2008).

^c Indicates compositions that exceed the SIMS matrix correction (Section 2.3). $\delta^{17,18}\text{O}$ values may have uncertainties that are higher than the reported values.

14 FeO-poor chondrules have coexisting olivine and pyroxene data, and their $\delta^{18}\text{O}$, $\delta^{17}\text{O}$, and $\Delta^{17}\text{O}$ values are similar, excluding relict grains (Fig. 7a–d). In addition, oxygen isotope ratios of coexisting phases in FeO-poor chondrules from LL3.0-3.2 chondrites, Acfer 094 (ungrouped C, 3.0), and Allende (CV3.6; Bonal et al., 2006) chondrites (Kita et al., 2010; Rudraswami et al., 2011; Ushikubo et al., 2012) are similar. Collectively, these measurements support existing petrologic evidence (i.e. textural and mineral/meso-stasis element partitioning relationships that match experimentally formed chondrules; Jones, 1994; Hewins, 1997) that many olivines and pyroxenes in FeO-poor chondrules crystallized co-magmatically.

When comparing the "host" $\delta^{18}\text{O}$ values within FeO-poor chondrules many pyroxenes are slightly ($\sim 1\%$) lower than coexisting olivines (Fig. 7a and b). Since $\Delta^{17}\text{O}$ values of these phases agree to within analytical precision (Fig. 7d), this shift in $\delta^{18}\text{O}$ from a 1:1 trend may be caused by mass dependent fractionation that exceeds the uncertainty of the instrumental bias correction ($\pm 0.5\%$; EA2). The equilibrium fractionation factors between olivine and pyroxene at high temperature (≥ 1200 °C) should be smaller than 0.5% , and $\delta^{18}\text{O}$ values in pyroxene should be higher than that of olivine (Clayton and Kieffer, 1991; Eiler, 2001). As olivine crystallizes at higher temperatures, relative to pyroxene, this indicates that the high-temperature

Table 2

Oxygen isotope ratios (‰), of relict grains within Yamato 81020 chondrules. Each row represents a single SIMS spot measurement.

Chondrule	Phase	Grain #	$\delta^{18}\text{O}$	Unc.	$\delta^{17}\text{O}$	Unc.	$\Delta^{17}\text{O}$	Unc.	Mg#
<i>Type I. Mg# >97</i>									
Y03	Olivine	1	−9.6	0.5	−12.9	0.2	−7.9	0.3	99.2
	Olivine	2	−9.2	0.5	−12.3	0.2	−7.5	0.3	99.1
Y19	Olivine	1	−11.6	0.4	−13.3	0.5	−7.2	0.5	99.1
Y22	Olivine	1	2.6	0.4	0.5	0.5	−0.8	0.5	99.3
	Olivine	2	2.4	0.4	0.9	0.5	−0.3	0.5	99.2
	Olivine	3	2.1	0.4	0.8	0.5	−0.3	0.5	99.2
	Olivine	4	1.9	0.4	0.8	0.5	−0.2	0.5	99.0
Y25	Olivine	1	−2.2	0.3	−4.6	0.4	−3.5	0.3	98.1
	Olivine	2	−8.4	0.3	−11.1	0.4	−6.8	0.3	99.5
	Olivine	3	0.9	0.3	−1.4	0.4	−1.9	0.3	99.5
Y71	Lpx	1	−2.7	0.5	−5.0	0.4	−3.6	0.4	97.7
Y74	Olivine	1	−7.9	0.3	−10.7	0.5	−6.6	0.4	98.9
<i>Type I. Mg# <97</i>									
Y12	Olivine	1	−0.8	0.3	−4.2	0.6	−3.8	0.6	94.9
	Olivine	2	−24.5	0.3	−26.8	0.6	−14.1	0.6	95.3
Y14	Olivine	1	−0.4	0.3	−4.1	0.4	−3.9	0.3	95.2
	Olivine	2	−1.4	0.3	−4.8	0.4	−4.1	0.3	95.2
	Lpx	3	−0.7	0.3	−5.1	0.4	−4.7	0.3	95.4
Y81	Olivine	1	−3.4	0.4	−6.7	0.6	−5.0	0.6	94.1
	Olivine	2	−3.2	0.4	−6.1	0.6	−4.4	0.6	94.0
	Lpx	3	−4.0	0.4	−7.1	0.6	−5.0	0.6	98.9
<i>Type II</i>									
Y2-09	Olivine	1	−3.1	0.5	−6.9	0.4	−5.3	0.4	93.9
	Olivine	2	−2.0	0.5	−6.5	0.4	−5.4	0.4	92.7
	Olivine	3	−2.2	0.5	−6.0	0.4	−4.9	0.4	71.0
	Olivine	4	−1.3	0.5	−6.0	0.4	−5.3	0.4	74.9
	Olivine	5	−1.6	0.5	−6.4	0.4	−5.6	0.4	95.2
Y2-14	Olivine	1, #1	−5.0	0.5	−8.5	0.4	−5.9	0.4	99.0
	Olivine	1, #2	−5.2	0.5	−8.3	0.4	−5.6	0.4	99.0
	Olivine	2	−0.8	0.5	−4.9	0.4	−4.5	0.4	60.3
Y28	Olivine	1	3.2	0.5	−0.2	0.4	−1.9	0.4	96.5
Y46	Olivine	1	−4.8	0.3	−7.5	0.6	−5.0	0.6	99.2
	Olivine	2	−18.5	0.3	−21.1	0.6	−11.4	0.6	78.0
Y58	Olivine	1	0.4	0.7	−2.7	0.3	−2.9	0.3	68.3
	Olivine	2	−2.6	0.7	−6.3	0.3	−4.9	0.3	75.7
	Olivine	3	1.3	0.7	−2.4	0.3	−3.1	0.3	61.8

Uncertainties are based on the 2SD values of bracketing measurements of S.C. olivine.

melt was slightly rich in heavier isotopes. This could have occurred through preferential evaporation of light O-isotopes, prior to olivine crystallization. After olivine crystallized, recondensation of light isotope enriched ambient gas, and/or kinetic isotope exchange between the chondrule melt and ambient gas could have resulted in light isotope enrichment of the melt during cooling (Libourel et al., 2006; Nagahara et al., 2008; Kita et al., 2010; Nagahara and Ozawa, 2012). In either scenario pyroxene crystallizing at a lower temperature would then be depleted in $\delta^{18}\text{O}$ when compared to olivine. If correct, the small size ($\sim 100\text{--}300\ \mu\text{m}$ dia.; EA4 and EA5) of the Y-80120 chondrules may have been more influenced by condensates/isotope exchange, when compared to larger chondrules from other chondrite groups, because of a higher surface area

to volume ratio. For instance, Rudraswami et al. (2011) demonstrate that coexisting olivine and pyroxene in 500–1200 μm sized FeO-poor Allende chondrules have no systematic shifts in $\delta^{18}\text{O}$. However, further high-precision oxygen isotope data from coexisting phases in chondrules are necessary to evaluate this hypothesis. Overall, the slight difference in oxygen isotope ratios between olivine and pyroxene does not detract from a strong indication that each phase crystallized from the final chondrule melt. It seems unlikely that a systematic $\sim 1\text{‰}$ difference in $\delta^{18}\text{O}$ between coexisting pyroxene and olivine (Fig. 7b), over a 5‰ range in $\Delta^{17}\text{O}$ (Fig. 7d), could occur if the majority of MgO-rich olivines in chondrules are relicts, as suggested by Libourel and Chaussidon (2011). Some olivines, and a few pyroxenes in FeO-poor Y-81020 chondrules clearly exhibit relict oxy-

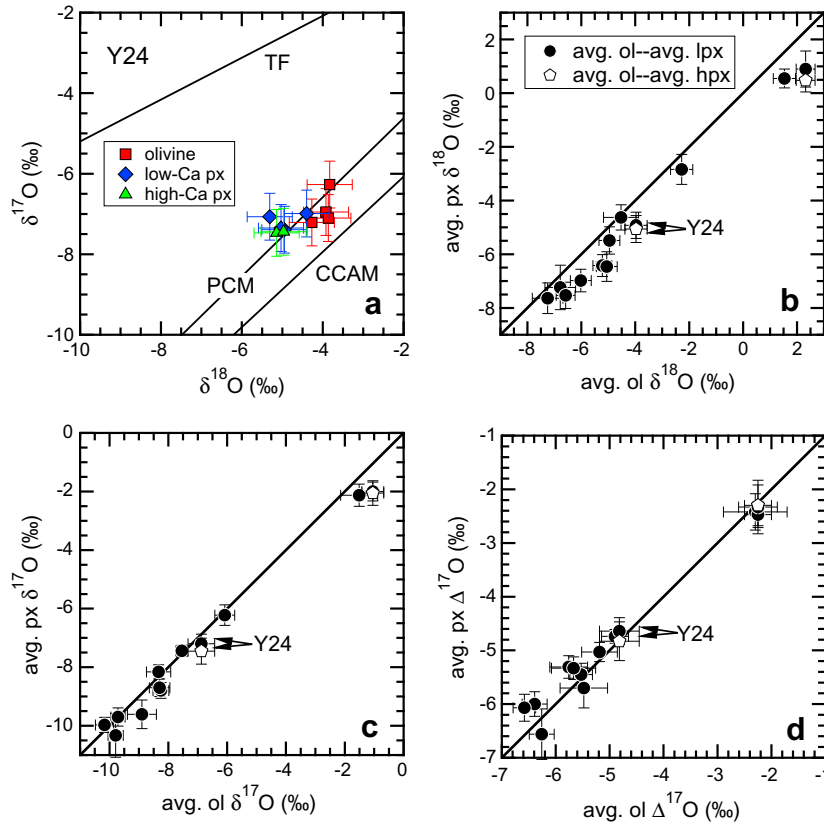


Fig. 7. Comparison of coexisting olivine and pyroxene oxygen isotope ratios in Y-81020 chondrules. Relict grains are excluded in the plots. (a) Example of “host” chondrule data used to determine averaged olivine and pyroxene O-isotope ratios. Uncertainties are the 2SD spot to spot reproducibility. (b–d) Comparison of averaged, coexisting olivine and pyroxene $\delta^{18}\text{O}$ (b), $\delta^{17}\text{O}$ (c), and $\Delta^{17}\text{O}$ (d) measurements in chondrules. A line indicating a 1:1 relationship is shown in Figs. b through d. Propagated uncertainties combine the spot to spot reproducibilities and the 2SE of measurements.

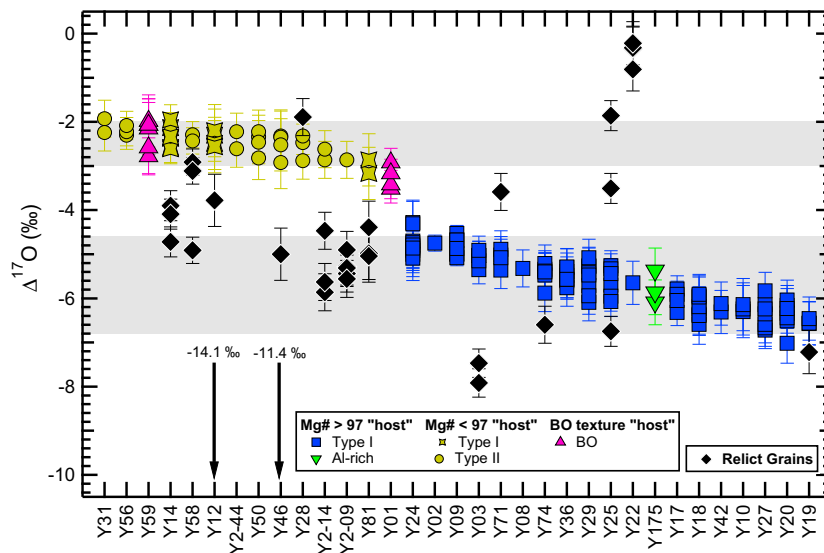


Fig. 8. Chondrule “host” and relict $\Delta^{17}\text{O}$ values. Each datum is a single SIMS spot measurement. Uncertainties are the 2SD spot to spot reproducibility, determined from bracketing measurements of S.C. olivine. Gray shaded regions represent the dominant $\Delta^{17}\text{O}$ “–2.5‰” and “–5.5‰” oxygen isotope reservoirs.

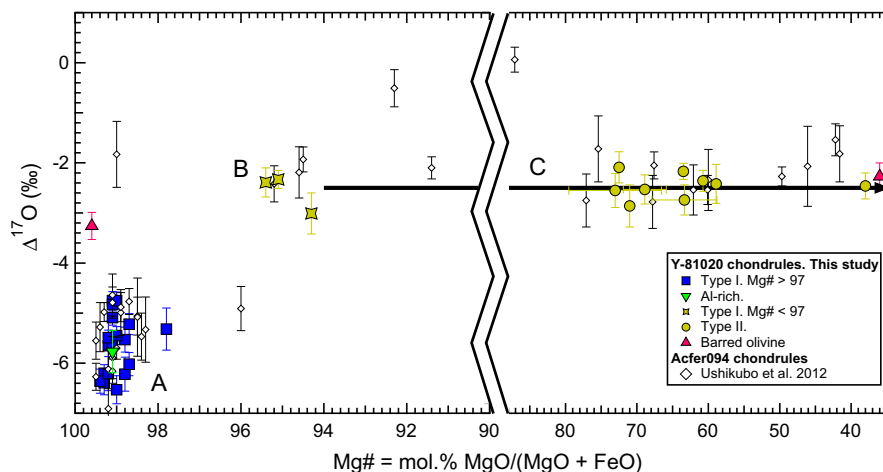


Fig. 9. Mg# of Y-81020 and Acfer 094 chondrules versus their “host” $\Delta^{17}\text{O}$ values, and interpretations of the chondrule-forming environment. Chondrule Mg# is calculated as the average of constituent olivine and/or low-Ca pyroxene Mg#'s. (A) Precursor material with a $\Delta^{17}\text{O}$ value of $\sim -5.5\text{‰}$, in an environment with limited dust enrichment ($100\times$ Solar) resulted in formation of Mg# >97 chondrules. The addition of positive $\Delta^{17}\text{O}$ H_2O ice to this precursor material, along with a potential increase in dust enrichment, aided in creating an oxidizing environment upon chondrule formation, yielding Mg# <97 type I chondrules with $\Delta^{17}\text{O}$ values of $\sim -2.5\text{‰}$ (B). Progressive dust/ice enrichment of the precursor material in (B) yielded even more oxidizing conditions, allowing for the formation of type II chondrules with a range of low Mg#'s (C). It is assumed that the anhydrous dust to ice ratio of precursors was constant in this environment, which yielded $\Delta^{17}\text{O}$ values of $\sim -2.5\text{‰}$ over a wide range of chondrule Mg#'s. Some precursors in (C) were Fe-rich, forming chondrules with extremely low Mg#'s. Acfer 094 chondrule data are from Ushikubo et al. (2012).

gen isotopic signatures (Table 2), but these are interspersed among other, co-magmatically crystallized olivine and pyroxene (Figs. 5 and 6).

5.3. Signatures of oxygen isotopic reservoirs within the CO chondrite forming region

The chondrules of Y-81020 indicate two dominant oxygen isotope reservoirs in the CO chondrite accretion region, as 19 of 33 yield an averaged “host” $\Delta^{17}\text{O}$ value of $-5.7 \pm 1.1\text{‰}$ (2SD) and 13 of 33 have a “host” $\Delta^{17}\text{O}$ value of $-2.5 \pm 0.5\text{‰}$ (2SD) (Fig. 8), henceforth referred to as the “ -5.5‰ ” and “ -2.5‰ ” reservoirs. Additionally, many relict grains have $\Delta^{17}\text{O}$ values near -5.5‰ or -2.5‰ (Fig. 8; Table 2).

In terms of “host” oxygen isotope ratios, chondrules with $\Delta^{17}\text{O}$ values near -5.5‰ are strictly limited to those with phenocryst Mg#'s greater than 97, while chondrules with $\Delta^{17}\text{O}$ values near -2.5‰ range in Mg# from 36 to 96 (Table 1; Fig. 9). This Mg# correlated bimodal distribution of oxygen isotope ratios is nearly identical to chondrules in the Acfer 094 (ungrouped C) chondrite (Ushikubo et al., 2012), where $\Delta^{17}\text{O} = -5.4 \pm 1.2\text{‰}$ chondrules are composed of Mg# >96 phenocrysts, and the majority of $\Delta^{17}\text{O} = -2.2 \pm 0.7\text{‰}$ chondrules consist of Mg# 43–96 phenocrysts (Fig. 9). Although Ushikubo et al. (2012) defined the oxygen isotope reservoirs as “ -5‰ ” and “ -2‰ ”, they are indistinguishable from the “ -5.5‰ ” and “ -2.5‰ ” reservoirs defined above, when considering uncertainties. In addition, chondrules with $\Delta^{17}\text{O}$ values near -5.5‰ and/or -2.5‰ are prominent features in CR, CV, CH, and CB_b chondrites (Krot et al., 2006a,b, 2010; Connolly and Huss, 2010; Libourel and Chaussidon, 2011; Nakashima et al., 2011; Rudraswami

et al., 2011; Schrader et al., 2013). $\Delta^{17}\text{O}$ values near -2.5‰ have also been measured in anhydrous IDP's (Aléon et al., 2009) and chondrule-like objects in cometary samples (McKeegan et al., 2006; Nakamura et al., 2008), and so these two oxygen isotope reservoirs may be widespread throughout the protoplanetary disk. Several type II chondrules have relict grains that are Mg-rich (Fig. 6) and with $\Delta^{17}\text{O}$ values lower than the “host” chondrule oxygen isotope ratios (Fig. 8). This relationship is consistent with petrographic observations and oxygen isotope measurements from other CO3.0 type II chondrules (Jones et al., 2000; Wasson et al., 2004; Kunihiro et al., 2004). Overall, the petrology and oxygen isotope characteristics of Y-81020 chondrules indicate that (1) multiple formation events occurred within a given environment, and (2) materials from $\Delta^{17}\text{O}$ “ -5.5‰ ” and “ -2.5‰ ” reservoirs were near each other, as phases (chiefly olivine) with signatures of one oxygen isotope reservoir can be found as relict grains in the other (Fig. 8).

Two chondrules, Y01 and Y59, have barred olivine textures (Fig. 4), indicative of total melting followed by rapid cooling (Tsuchiyama et al., 1980, 2004; Clayton et al., 1983; Lofgren and Lanier, 1990). Oxygen isotope ratios of olivine in these chondrules are homogeneous within the precision of SIMS analyses. Y01 contains Mg# 99.6 olivine, and has a $\Delta^{17}\text{O}$ of -3.3‰ (Table 1). This value is intermediate when compared to the measured oxygen isotope ratios of Mg# >97 and Mg# <97 porphyritic/Al-rich chondrules, and could indicate a minor oxygen isotope reservoir within the CO chondrite accretion region. Alternatively, it could represent an FeO-rich chondrule that remelted in an isotopic environment that produced FeO-poor chondrules, and exchanged oxygen, but not other elements. Y59 is a type II BO chondrule with a $\Delta^{17}\text{O}$ of -2.3‰ (Table 1), which

is consistent with the “host” oxygen isotope ratios of the type II PO chondrules/fragments.

Several chondrules contain grains that we have defined as “relicts”, and they have unique oxygen isotope ratios (Table 2; Fig. 8). Chondrule Y22 contains 4 relict olivine grains with an average $\Delta^{17}\text{O}$ of $-0.4 \pm 0.3\text{‰}$ (2SE). Similar $\Delta^{17}\text{O}$ values have been reported from a type I olivine fragment in Acfer 094 (Ushikubo et al., 2012), some BO chondrules in CV3 chondrites (Clayton et al., 1983; Jones et al., 2004; Rudraswami et al., 2011), and some type II chondrules in CR2 chondrites (Connolly and Huss, 2010; Schrader et al., 2013). The $\Delta^{17}\text{O} -0.4\text{‰}$ signature could represent an additional oxygen isotope reservoir in the carbonaceous chondrite forming region, or could indicate a variation in mixing of ^{16}O -rich and ^{16}O -poor precursor material (relative to materials mixed in other precursors) as suggested by Jones et al. (2004). Chondrules Y12, Y46, Y03, and Y19 have relict olivines that are significantly ^{16}O -rich ($\Delta^{17}\text{O}$: -7.2‰ to -14.1‰) (Fig. 8), which could suggest that they formed in a CAI/AOA oxygen isotope reservoir ($\Delta^{17}\text{O} < -20\text{‰}$; Yurimoto et al., 2008). Perhaps through multiple generations of chondrule heating events these relict grains became depleted in ^{16}O , relative to CAIs. Alternatively, the ^{16}O -rich relict domains could be very small within grains, meaning that the SIMS spot analyses sampled a mixture of relict and host material, yielding intermediate $\Delta^{17}\text{O}$ values.

5.4. Implications of two oxygen isotope reservoirs in the CO chondrite accretion region

The relationship between oxygen isotope ratios and Mg#’s of Y-81020 chondrules signifies the existence of variables that affected both the oxidation state and the oxygen isotope ratio of a given chondrule-forming environment. The high Mg# (>97) of the $\Delta^{17}\text{O} \sim -5.5\text{‰}$ chondrules suggests formation in a relatively reduced environment, with $\log f_{\text{O}_2}$ values less than IW-2 (Kring, 1988; Zanda et al., 1994). The lower Mg#’s (<97) of the $\Delta^{17}\text{O} \sim -2.5\text{‰}$ chondrules, however, indicate that conditions were more oxidizing and that the oxygen isotope ratio of precursor material was ^{16}O -poor when compared to the Mg# >97 chondrules. Overall, these results are analogous to those from CR2 chondrites, in which type II chondrules have $\Delta^{17}\text{O}$ values that are more positive (-2.0‰ to $+1.1\text{‰}$; Krot et al., 2006b; Connolly and Huss, 2010; Schrader et al., 2013) than type I chondrules (0‰ to -6‰ ; Krot et al., 2006b; Scharder et al. (2013)). In the case of Y-81020, more oxidized chondrules show a wide range in Mg# (96–36), yet have essentially the same oxygen isotope ratios (Fig. 9). What variables could have led to such observations? Similar to interpretations from Connolly and Huss (2010) and Scharder et al. (2013), we suspect that three factors, the degree of dust enrichment relative to the bulk Solar System, the bulk Fe content of precursor material, and the amount of H_2O in precursors, could explain both variation in Mg# and the presence of two distinct oxygen isotopic reservoirs.

Ebel and Grossman (2000) used multiple, thermodynamic based crystallization models, including CMAS melting (Berman, 1983), VAPORS (Ebel et al., 2000), and MELTS (Ghiorso and Sack, 1995) to determine the effect

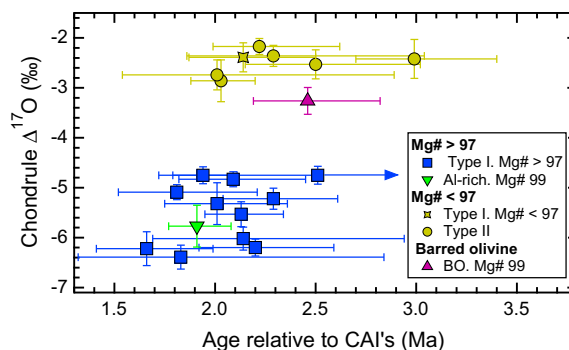


Fig. 10. ^{26}Al ages of Y-81020 chondrules (relative to CAIs) as a function of $\Delta^{17}\text{O}$. Relative age determinations are from Kurahashi et al. (2008), and assume a ^{26}Al half-life of 0.73 Ma, and an initial ($^{26}\text{Al}/^{27}\text{Al}$) CAI ratio of 5×10^{-5} .

of dust enrichment on the oxygen fugacity of CI chondrite analog compositions, and also the effect on phase compositions as chondrules cooled from high temperatures. From 900 to 2100 °C their model predicts oxygen fugacities of IW-3.1, IW-1.7, and IW-1.3 at dust enrichments of 100, 500, and 1000 times that of the Solar abundance, respectively. At these dust enrichments, Ebel and Grossman (2000) predict that olivines that crystallize from melt at 10^{-3} bar will have Mg#’s of 97.5, 86, and 69, respectively. The model also predicts that, in general, late-stage (i.e. low temperature) melts increase in SiO_2 , FeO , and Na_2O , and decrease in Al_2O_3 , MgO , and CaO when CI dust enrichment increases from 100 to 1000× Solar System. Such trends are broadly observed when comparing mesostasis compositions of magnesian and ferroan chondrules in Y-81020 (EA6). Collectively, these results suggest that Mg# >97 chondrules likely formed in an environment with $\sim 100\times$ Solar System CI dust enrichment, and that higher dust densities likely aided in the formation of Mg# 96–36 chondrules in Y-81020.

However, dust enrichment alone may not be able to account for the extremely FeO-rich chondrules, and so it is likely that some Mg# <97 chondrules were formed from precursors that were Fe-rich, relative to the materials that formed Mg# >97 chondrules. Using the Fe contents in phases (including metals and sulfides) and their respective calculated volume ratios, Kurahashi (2006) estimated bulk Fe concentrations of 5–15 wt.% in type I Y-81020 chondrules. In contrast, type II chondrules Y31, Y50, and Y56, which consist almost entirely of olivine, have total Fe contents of 19, 38, and 25 wt.%, respectively, when calculated with respective olivine EPMA data (EA6). The variability in the bulk Fe content of precursor material, either as an alloy, a sulfide, and/or as FeO-bearing silicates, does not have an effect on oxygen isotope ratios, as Mg# 96–36 chondrules are nearly constant in $\Delta^{17}\text{O}$ (Fig. 9).

Finally, the abundance of H_2O in precursors could explain the existence of two distinct oxygen isotope reservoirs. This is because measurements of chondritic H_2O are typically ^{16}O -poor when compared to the bulk chondritic value (Choi et al., 1998; Sakamoto et al., 2007; Yurimoto et al., 2008). If indeed ^{16}O -poor H_2O were added to precursors,

one would expect the formation of chondrules with more positive $\Delta^{17}\text{O}$ values, especially considering that H_2O vapor readily exchanges its oxygen isotopes with molten silicate (Yu et al., 1995). In addition, H_2O is an oxidizing agent (Fedkin and Grossman, 2006; Grossman et al., 2008), meaning that its addition to precursors would have contributed to the formation of FeO-rich chondrules.

Considering the effect of oxidation state and oxygen isotope ratios as a function of dust and H_2O enrichment we envision that the CO chondrule-forming region was predominantly divided into three environments (Fig. 9). The first environment was limited in CI dust enrichment ($100\times$ Solar System), which yielded reducing conditions upon transient heating, and produced chondrules with metal alloys and $\text{Mg}\# > 97$ olivines and pyroxenes, with “host” $\Delta^{17}\text{O}$ values of -4.5 to -6.5‰ (Fig. 9A). The second environment was similar to the first, except that cooler ambient temperatures prevailed (<150 K; Lewis, 1972), allowing for H_2O ice with a positive $\Delta^{17}\text{O}$ to condense and then incorporate into chondrule precursors. The addition of H_2O would have induced more oxidized conditions during heating, and repeated brief heating events would have allowed for the ^{16}O -poor H_2O to exchange its isotopes with newly-formed chondrules in their molten state (Yu et al., 1995). Precursors may also have been more enriched in CI dust, which would have contributed to more oxidized chondrule-forming conditions. Overall, this environment led to the formation of $\text{Mg}\# \sim 95$ chondrules with “host” $\Delta^{17}\text{O}$ values near -2.5‰ (Fig. 9B). The third environment was similar to the second in that precursor material had a similar ratio of H_2O to anhydrous components, but it is likely that there was a greater abundance of bulk Fe. The total dust enrichment was also significantly enhanced, perhaps as high as $1000\times$ Solar System and thereby induced an even more oxidized environment. This facilitated the formation of type II chondrules with a wide range of $\text{Mg}\#$'s but a constant $\Delta^{17}\text{O}$ of $\sim -2.5\text{‰}$ (Fig. 9C). We emphasize that even if the original H_2O had extremely ^{16}O -poor components, similar to those found in cosmic symplectites ($\Delta^{17}\text{O}$: $+80\text{‰}$; Sakamoto et al., 2007), the constant $\Delta^{17}\text{O}$ value among the $\text{Mg}\#$ 36–96 chondrules (Fig. 9) indicates that such extreme ^{16}O -depleted water would have been homogenized in the precursor, albeit in small amounts, prior to the final chondrule formation period.

Overall, the $\Delta^{17}\text{O}/\text{Mg}\#$ relationships of Y-81020, Acfer 094 (Ushikubo et al., 2012), and CR2 chondrules (Krot et al., 2006b; Connolly and Huss, 2010; Schrader et al., 2013) suggest similar variables that influenced their formation within respective environments. The overlap in $\Delta^{17}\text{O}$ between respective FeO-poor and FeO-rich chondrules could indicate sampling of common physicochemical systems among carbonaceous chondrite subtypes, but more work is necessary to fully assess this hypothesis.

5.5. Relative chondrule ages versus $\Delta^{17}\text{O}$ in Y-81020

The implication that the CO chondrule-forming environment consisted of distinct domains of precursors leads to the question of whether there was a spatial separation over the course of chondrule production, or whether the

environment evolved with time. Such inferences place constraints on the timescale, location, and migration of the snow line within the CO chondrite accretion region (e.g. Ciesla and Cuzzi, 2006). Combining the oxygen isotope measurements of chondrules with corresponding Al–Mg measurements (Kurahashi et al., 2008) we find that $\text{Mg}\# > 97$, $\Delta^{17}\text{O} \sim -5.5\text{‰}$ (excluding BO chondrule Y01) and $\text{Mg}\#$ 96–36, $\Delta^{17}\text{O} \sim -2.5\text{‰}$ chondrules have relative ages of 1.7–2.5 and 2.0–3.0 Ma, respectively, after the formation of CAIs. The similarities in relative ages, when combined with uncertainties, indicate that $\Delta^{17}\text{O} \sim -5.5\text{‰}$ and $\sim -2.5\text{‰}$ chondrules formed contemporaneously within the CO chondrite accretion region (Fig. 10). This interpretation is strengthened by the fact that $\Delta^{17}\text{O} \sim -2.5\text{‰}$ chondrules contain $\Delta^{17}\text{O} \sim -5.5\text{‰}$ relict grains, and that $\Delta^{17}\text{O} \sim -5.5\text{‰}$ chondrules have $\Delta^{17}\text{O} \sim -2.5\text{‰}$ relict grains (Fig. 8). Collectively, this implies that the snowline was spatially fixed during the course of chondrule formation, and separated the CO chondrite accretion region into two volumes. Located within the region of ice condensation was $\Delta^{17}\text{O} \sim -2.5\text{‰}$ precursor material and all of its attributes (high dust enrichment, increased total Fe, increased amounts of H_2O incorporated into precursors, and oxidized chondrule-forming conditions). This environment could have been radially and/or vertically adjacent to the low dust enrichment and more reduced $\Delta^{17}\text{O} \sim -5.5\text{‰}$ chondrule-forming region (Cassen, 2001; Ciesla and Cuzzi, 2006).

6. CONCLUSIONS

- (1) In chondrules where oxygen isotopes were measured in both olivine and pyroxene, many olivine grains are similar to coexisting pyroxene grains, suggesting comagmatic crystallization. However, several chondrules also contain relict olivine and pyroxene grains with unique oxygen isotope signatures.
- (2) Yamato 81020 chondrules exhibit a prominent bimodal distribution in oxygen isotope ratios. Those containing olivine and/or pyroxene phenocrysts with $\text{Mg}\#$'s greater than 97 have “host” $\Delta^{17}\text{O}$ values ranging from -4.8‰ to -6.5‰ . Chondrules with olivine and/or pyroxene phenocrysts that have $\text{Mg}\#$'s less than 97 have “host” $\Delta^{17}\text{O}$ values ranging from -2.1‰ to -3.0‰ . An $\text{Mg}\#$ 99.6 BO chondrule has a “host” $\Delta^{17}\text{O}$ value of -3.3‰ .
- (3) The existence of $\Delta^{17}\text{O}$ “ -5.5‰ ” and “ -2.5‰ ” oxygen isotope reservoirs in the CO chondrite accretion region is explained in the following way: the “ -5.5‰ ” reservoir was likely a region of limited dust enrichment ($100\times$ Solar System), which produced reducing transient heating conditions that formed $\text{Mg}\# > 97$ chondrules. The $\Delta^{17}\text{O}$ “ -2.5‰ ” reservoir was likely cooler at ambient temperature (<150 K), allowing for the addition of H_2O ice to precursors which then isotopically homogenized during chondrule formation. The inferred positive $\Delta^{17}\text{O}$ value of H_2O , along with the propensity for H_2O to readily exchange O-isotopes with molten silicate resulted in the formation of chondrules with $\Delta^{17}\text{O}$ values near

–2.5‰. In addition to the oxidizing nature of H₂O addition upon transient heating, increased dust enrichment and/or Fe abundances of precursors aided in producing Mg# 96–36 chondrules. The relative ages from chondrules indicate that the Δ¹⁷O “–5.5‰” and “–2.5‰” reservoirs existed contemporaneously, suggesting that the snow line was spatially fixed over the timescale of chondrule formation, and only overlapped a limited volume within the CO chondrite accretion region. Mixing of materials from either side of the snow line would then have been necessary in order to accrete the CO parent body.

ACKNOWLEDGMENTS

Authors acknowledge H. Kojima and K. Misawa, NIPR, for use of Y81020 thin sections for this study, Daisuke Nakashima for discussion, Jim Kern for instrumental support. Helpful comments from Rhian Jones, Tak Kunihiro, Associate editor Sasha Krot, and an anonymous reviewer, significantly improved the manuscript. This work is supported by NASA Cosmochemistry Program (NNX10AH77G and NNX11AG62G, N.K.). WiscSIMS is partly supported by NSF (EAR10-53466).

APPENDIX A. SUPPLEMENTARY DATA

Supplementary data associated with this article can be found, in the online version, at <http://dx.doi.org/10.1016/j.gca.2012.10.034>.

REFERENCES

- Airieu S. A., Farquhar J., Thiemens M. H., Leshin L. A., Bao H. and Young E. (2005) Planetary sulfate and aqueous alteration in CM and CI carbonaceous chondrites. *Geochim. Cosmochim. Acta* **69**, 4166–4171.
- Aléon J., Engrand C., Leshin L. A. and McKeegan K. D. (2009) Oxygen isotopic composition of chondritic interplanetary dust particles: a genetic link between carbonaceous chondrites and comets. *Geochim. Cosmochim. Acta* **73**, 4558–4575.
- Amelin Y., Krot A. N., Hutcheon I. D. and Ulyanov A. A. (2002) Lead isotopic ages of chondrules and calcium–aluminum-rich inclusions. *Science* **297**, 1678–1683.
- Amelin Y., Kaltenbach A., Iizuka T., Stirling C. H., Ireland T. R., Petaev M. and Jacobsen S. B. (2010) U–Pb chronology of the Solar System’s oldest solids with variable ²³⁸U/²³⁵U. *Earth Planet. Sci. Lett.* **300**, 343–350.
- Baertschi P. (1976) Absolute ¹⁸O content of standard mean ocean water. *Earth Planet. Sci. Lett.* **31**, 341–344.
- Baker L., Franchi I. A., Wright I. P. and Pillinger C. T. (2002) The oxygen isotopic composition of water from Tagish Lake: its relationship to low-temperature phases and to other carbonaceous chondrites. *Meteorit. Planet. Sci.* **37**, 977–985.
- Benedix G. K., Leshin L. A., Farquhar J., Jackson T. and Thiemens M. H. (2003) Carbonates in CM2 chondrites: constraints on alteration conditions from oxygen isotopic compositions and petrographic observations. *Geochim. Cosmochim. Acta* **67**, 1577–1588.
- Berman R. G. (1983) A thermodynamic model for multicomponent melts, with application to the system CaO–MgO–Al₂O₃–SiO₂. Ph. D. thesis, Univ. British Columbia.
- Berlin J., Jones R. H. and Brearley A. J. (2011) Fe–Mn systematics of type IIA chondrules in unequilibrated CO, CR, and ordinary chondrites. *Meteorit. Planet. Sci.* **46**, 513–533.
- Boesenberg J. S., Cosarinsky M., McKeegan K. D., Chaussidon M. and Hewins R. H. (2007) An experimental study of Fe–Mg and oxygen isotope exchange between relict olivine and chondrule melt. *Lunar Planet. Sci. XXXVIII*. Lunar Planet. Inst., Houston. #1621 (abstr.).
- Bonal L., Quirico E., Bourot-Denise M. and Montagnac G. (2006) Determination of the petrologic type of CV3 chondrites by Raman spectroscopy of included organic matter. *Geochim. Cosmochim. Acta* **70**, 1849–1863.
- Cassen P. (2001) Nebular thermal evolution and the properties of primitive planetary materials. *Meteorit. Planet. Sci.* **36**, 671–700.
- Chakraborty S. (2010) Diffusion coefficients in olivine, wadsleyite, and ringwoodite. In *Reviews in Mineralogy and Geochemistry*, vol. 72 (eds. Y. Zhang and D. J. Cherniak). Mineralogical Society of America, Washington, D.C., pp. 603–639.
- Choi B. G., McKeegan K. D., Krot A. N. and Wasson J. T. (1998) Extreme oxygen-isotope compositions in magnetite from unequilibrated ordinary chondrites. *Nature* **392**, 577–579.
- Choi B. G., Krot A. N. and Wasson J. T. (2000) Oxygen isotopes in magnetite and fayalite in CV chondrites Kaba and Mokoia. *Meteorit. Planet. Sci.* **35**, 1239–1248.
- Ciesla F. J. and Cuzzi J. N. (2006) The evolution of the water distribution in a viscous protoplanetary disk. *Icarus* **181**, 178–204.
- Clayton R. N. (1993) Oxygen isotopes in meteorites. *Annu. Rev. Earth Planet. Sci.* **21**, 115–149.
- Clayton R. N. (2002) Solar System – self-shielding in the Solar nebula. *Nature* **415**, 860–861.
- Clayton R. N. and Kieffer S. W. (1991) Oxygen isotopic thermometer calibrations. In *Stable Isotope Geochemistry: A Tribute to Samuel Epstein*, vol. 3 (eds. Jr. H. P. Taylor, J. R. O’Neil and I. R. Kaplan). Geochim. Soc. Spec. Publ., pp. 3–10.
- Clayton R. N., Grossman L. and Mayeda T. K. (1973) Component of primitive nuclear composition in carbonaceous meteorites. *Science* **182**, 485–488.
- Clayton R. N., Onuma N., Grossman L. and Mayeda T. K. (1977) Distribution of pre-solar component in Allende and other carbonaceous chondrites. *Earth Planet. Sci. Lett.* **34**, 209–224.
- Clayton R. N., Onuma N., Ikeda Y., Mayeda T. K., Hutcheon I. D., Olsen E. J. and Molini-Velso C. (1983) Oxygen isotopic compositions of chondrules in Allende and ordinary chondrites. In *Chondrules and Their Origins* (ed. E. A. King). Lunar Planet. Inst., Houston, pp. 37–43.
- Clayton R. N., Mayeda T. K. and Rubin A. E. (1984) Oxygen isotopic compositions of enstatite chondrites and aubrites. *J. Geophys. Res.* **89**, C245–C249.
- Clayton R. N., Mayeda T. K., Goswami J. N. and Olsen E. J. (1991) Oxygen isotope studies of ordinary chondrites. *Geochim. Cosmochim. Acta* **55**, 2317–2337.
- Cole D. R. and Chakraborty S. (2001) Rates and mechanisms of isotope exchange. In *Reviews in Mineralogy and Geochemistry*, vol. 43 (eds. J. W. Valley and D. R. Cole). Mineralogical Society of America, Washington, D.C., pp. 83–223.
- Connelly J. N., Amelin Y., Krot A. N. and Bizarro M. (2008) Chronology of the Solar System’s oldest solids. *Astrophys. J.* **675**, L121–L124.
- Connolly, Jr., H. C. and Huss G. R. (2010) Compositional evolution of the protoplanetary disk: oxygen isotopes of type-II chondrules from CR2 chondrites. *Geochim. Cosmochim. Acta* **74**, 2473–2483.

- Connolly, Jr., H. C., Hewins R. H., Ash R. D., Zanda B., Lofgren G. E. and Bourrot-Denise M. (1994) Carbon and the formation of reduced chondrules. *Nature* **371**, 136–139.
- Ebel D. S. and Grossman L. (2000) Condensation in dust-enriched systems. *Geochim. Cosmochim. Acta* **64**, 339–366.
- Ebel D. S., Ghiorso M. S., Sack R. O. and Grossman L. (2000) Gibbs energy minimization in gas plus liquid plus solid systems. *J. Comput. Chem.* **21**, 247–256.
- Eiler J. M. (2001) Oxygen isotope variations of basaltic lavas and upper mantle rocks. In *Stable Isotope Geochemistry*, vol. 43 (eds. J. W. Valley and D. R. Cole). Mineralogical Society of America, Washington, D.C., pp. 319–364.
- Fedkin A. V. and Grossman L. (2006) The fayalite content of chondritic olivine: obstacle to understanding the condensation of rocky material. In *Meteorites and the Early Solar System II* (eds. D. S. Lauretta and H. Y. McSween). Univ. of Arizona Press, Tuscon, pp. 279–294.
- Gerard O. and Jaoul O. (1989) Oxygen diffusion in San-Carlos olivine. *J. Geophys. Res.* **94**, 4119–4128.
- Ghiorso M. S. and Sack R. O. (1995) Chemical mass-transfer in magmatic processes. 4. A revised and internally consistent thermodynamic model for the interpolation and extrapolation of liquid–solid equilibria in magmatic systems at elevated-temperatures and pressures. *Contrib. Mineral. Petrol.* **119**, 197–212.
- Goodrich C. A., Kita N. T., Spicuzza M. J., Valley J. W., Zipfel J., Mikouchi T. and Miyamoto M. (2010) The Northwest Africa 1500 meteorite: not a urelite, maybe a brachinite. *Meteorit. Planet. Sci.* **45**, 1906–1928.
- Greenwood J. P. and Hess P. C. (1996) Congruent melting kinetics: constraints on chondrule formation. In *Chondrules and the Protoplanetary Disk* (eds. R. H. Hewins, R. H. Jones and E. R. D. Scott). Cambridge Univ. Press, Cambridge, pp. 205–211.
- Grossman J. N. (1988) Formation of chondrules. In *Meteorites and the Early Solar System* (eds. J. F. Kerridge and M. S. Matthews). Univ. of Arizona Press, Tuscon, pp. 680–696.
- Grossman J. N. and Brearley A. J. (2005) The onset of metamorphism in ordinary and carbonaceous chondrites. *Meteorit. Planet. Sci.* **40**, 87–122.
- Grossman L., Beckett J. R., Fedkin A. V., Simon S. B. and Ciesla F. J. (2008) Redox conditions in the Solar nebula: observational, experimental, and theoretical constraints. In *Reviews in Mineralogy and Geochemistry*, vol. 68 (ed. G. J. MacPherson). Mineralogical Society of America, Washington, D.C., pp. 93–140.
- Heck P. R., Ushikubo T., Schmitz B., Kita N. T., Spicuzza M. J. and Valley J. W. (2010) A single asteroidal source for extraterrestrial Ordovician chromite grains from Sweden and China: high-precision oxygen three-isotope SIMS analysis. *Geochim. Cosmochim. Acta* **74**, 497–509.
- Hewins R. H. (1991) Retention of sodium during chondrule melting. *Geochim. Cosmochim. Acta* **45**, 935–942.
- Hewins R. H. (1997) Chondrules. *Annu. Rev. Earth Planet. Sci.* **25**, 61–83.
- Hewins R. H. and Radomsky P. M. (1990) Temperature conditions for chondrule formation. *Meteoritics* **25**, 309–318.
- Hewins R. H., Connolly, Jr., H. C., Lofgren G. E. and Libourel G. (2005) Experimental constraints on chondrule formation. In *Chondrites and the Protoplanetary Disk, ASP Conference Series*, vol. 341 (eds. A. N. Krot, E. R. Scott and B. Reipurth). Astron. Soc. Pacific, San Francisco, pp. 286–317.
- Hsu W., Guan Y., Hua X., Wang Y., Leshin L. and Sharp T. G. (2005) Aqueous alteration of opaque assemblages in the Ningqiang carbonaceous chondrite: evidence from oxygen isotopes. *Earth Planet. Sci. Lett.* **243**, 107–114.
- Huss G. R., MacPherson G. J., Wasserburg G. J., Russell S. S. and Srinivasan G. (2001) Aluminum-26 in calcium–aluminum-rich inclusions and chondrules from unequilibrated ordinary chondrites. *Meteorit. Planet. Sci.* **36**, 975–997.
- Hutcheon I. D., Marhas K. K., Krot A. N., Goswami J. N. and Jones R. H. (2009) ²⁶Al in plagioclase-rich chondrules in carbonaceous chondrites: evidence for an extended duration of chondrule formation. *Geochim. Cosmochim. Acta* **73**, 5080–5099.
- Johnson C. A. and Prinz M. (1991) Chromite and olivine in type-II chondrules in carbonaceous and ordinary chondrites- implications for thermal histories and group-differences. *Geochim. Cosmochim. Acta* **55**, 893–904.
- Jones R. H. (1990) Petrology and mineralogy of type-II FeO-rich chondrules in Semarkona (LL3.0) – origin by closed-system fractional crystallization, with evidence for supercooling. *Geochim. Cosmochim. Acta* **54**, 1785–1802.
- Jones R. H. (1992) On the relationship between isolated and chondrule olivine grains in the carbonaceous chondrite ALHA77307. *Geochim. Cosmochim. Acta* **56**, 467–482.
- Jones R. H. (1994) Petrology of FeO-poor, porphyritic pyroxene chondrules in the Semarkona chondrite. *Geochim. Cosmochim. Acta* **58**, 5325–5340.
- Jones R. H. (1996) FeO-rich porphyritic pyroxene chondrules in unequilibrated ordinary chondrites. *Geochim. Cosmochim. Acta* **60**, 3115–3138.
- Jones R. H. (2012) Petrographic constraints on the diversity of chondrule reservoirs in the protoplanetary disk. *Meteorit. Planet. Sci.* **47**, 1176–1190.
- Jones R. H. and Scott E. R. D. (1989) Petrology and thermal history of type IA chondrules in the Semarkona (LL3.0) chondrite. *Proc. Lunar Planet. Sci. Conf.* **19**, 523–536.
- Jones R. H., Saxton J. M., Lyon I. C. and Turner G. (2000) Oxygen isotopes in chondrule olivine and isolated olivine grains from the CO3 chondrite Allan Hills A77307. *Meteorit. Planet. Sci.* **35**, 849–857.
- Jones R. H., Leshin L. A., Guan Y. B., Sharp Z. D., Durakiewicz T. and Schilk A. J. (2004) Oxygen isotope heterogeneity in chondrules from the Mokoia CV3 carbonaceous chondrite. *Geochim. Cosmochim. Acta* **68**, 3423–3438.
- Kallemeyn G. W., Rubin A. E. and Wasson J. T. (1994) The compositional classification of chondrites. VI. The CR carbonaceous chondrite group. *Geochim. Cosmochim. Acta* **58**, 2873–2888.
- Kimura M., Grossman J. N. and Weisberg M. K. (2008) Fe–Ni metal in primitive chondrites: indicators of classification and metamorphic conditions for ordinary and CO chondrites. *Meteorit. Planet. Sci.* **43**, 1161–1177.
- Kita N. T. and Ushikubo T. (2012) Evolution of protoplanetary disk inferred from ²⁶Al chronology of individual chondrules. *Meteorit. Planet. Sci.* **47**, 1108–1119.
- Kita N. T., Nagahara H., Togashi S. and Morshita Y. (2000) A short duration of chondrule formation in the Solar nebula: evidence from ²⁶Al in Semarkona ferromagnesian chondrules. *Geochim. Cosmochim. Acta* **64**, 3913–3922.
- Kita N. T., Ushikubo T., Fu B. and Valley J. W. (2009) High precision SIMS oxygen isotope analysis and the effect of sample topography. *Chem. Geol.* **264**, 43–57.
- Kita N. T., Nagahara H., Tachibana S., Tomomura S., Spicuzza M. J., Fournelle J. H. and Valley J. W. (2010) High precision SIMS oxygen three isotope study of chondrules in LL3 chondrites: role of ambient gas during chondrule formation. *Geochim. Cosmochim. Acta* **74**, 6610–6635.
- Kojima T., Yada S. and Tomeoka K. (1995) Ca–Al-rich inclusions in three Antarctic CO3 chondrites, Yamato-81020, Yamato-82050 and Yamato-790992: record of low-temperature alteration. In *19th NIPR Symp. Antarctic Meteorites*, vol. 8. pp. 79–96.

- Kring D. A. (1988) The petrology of meteoritic chondrules: evidence for fluctuating conditions in the Solar nebula. Ph. D. thesis, Harvard Univ.
- Krot A. N., Yurimoto H., McKeegan K. D., Leshin L., Chaussidon M., Libourel G., Yoshitake M., Huss G. R., Guan Y. and Zanda B. (2006a) Oxygen isotopic compositions of chondrules: implications for evolution of oxygen isotopic reservoirs in the inner Solar nebula. *Chem. Erde* **66**, 249–276.
- Krot A. N., Libourel G. and Chaussidon M. (2006b) Oxygen isotope compositions of chondrules in CR chondrites. *Geochim. Cosmochim. Acta* **70**, 767–779.
- Krot A. N., Nagashima K., Yoshitake M. and Yurimoto H. (2010) Oxygen isotopic compositions of chondrules from the metal-rich chondrites Isheyevo (CH/CB_b), MAC 02675 (CB_b) and QUE 94627 (CB_b). *Geochim. Cosmochim. Acta* **74**, 2190–2211.
- Krot A., Hutcheon I., Nagashima K., Crites S., Gasda P., Hallis L., Jilly C., Petaev M., Robertson H., Taylor G. and Telus M. (2011) Origin of ferroan olivine in matrices of unequilibrated chondrites. *Meteorit. Planet. Sci.* **46**, A131 (abstr.).
- Kunihiro T., Rubin A. E., McKeegan K. D. and Wasson J. T. (2004) Oxygen-isotopic compositions of relict and host grains in the Yamato 81020 CO3.0 chondrite. *Geochim. Cosmochim. Acta* **68**, 3599–3606.
- Kurahashi E. (2006) Evolution of solid materials in the protoplanetary disk: constraints from ²⁶Al ages and cosmochemical properties of chondrules in a primitive CO chondrite. Ph. D. thesis, Tokyo Univ.
- Kurahashi E., Kita N. T., Nagahara H. and Morishita Y. (2008) ²⁶Al–²⁶Mg systematics of chondrules in a primitive CO chondrite. *Geochim. Cosmochim. Acta* **72**, 3865–3882.
- Larimer J. W. (1975) The effect of C/O ratio on the condensation of planetary material. *Geochim. Cosmochim. Acta* **39**, 389–392.
- Larimer J. W. and Bartholomay M. (1979) Role of carbon and oxygen in cosmic gases—some applications to the chemistry and mineralogy of enstatite chondrites. *Geochim. Cosmochim. Acta* **43**, 1455–1466.
- Lewis J. S. (1972) Low-temperature condensation from the Solar nebula. *Icarus* **16**, 241–252.
- Libourel G. and Chaussidon M. (2011) Oxygen isotopic constraints on the origin of Mg-rich olivines from chondritic meteorites. *Earth Planet. Sci. Lett.* **301**, 9–21.
- Libourel G., Krot A. N. and Tissandier L. (2006) Role of gas–melt interaction during chondrule formation. *Earth Planet. Sci. Lett.* **251**, 232–240.
- Lofgren G. and Lanier A. B. (1990) Dynamic crystallization study of barred olivine chondrules. *Geochim. Cosmochim. Acta* **54**, 3537–3551.
- Lyons J. R. and Young E. D. (2005) CO self-shielding as the origin of oxygen isotope anomalies in the early Solar nebula. *Nature* **435**, 317–320.
- McKeegan K. D., Leshin L. A., Russell S. S. and MacPherson G. J. (1998) Oxygen isotopic abundances in calcium–aluminum-rich inclusions from ordinary chondrites: implications for nebular heterogeneity. *Science* **280**, 414–418.
- McKeegan K. D., Aléon J., Bradley J., Brownlee D., Busemann H., Butterworth A., Chaussidon M., Fallon S., Floss C., Gilmour J., Gounelle M., Graham G., Guan Y., Heck P. R., Hoppe P., Hutcheon I. D., Huth J., Ishii H., Ito M., Jacobsen S. B., Kearsley A., Leshin L. A., Liu M.-C., Lyon I., Marhas K., Marty B., Maraj G., Meibom A., Messenger S., Mostefaoui S., Mukhopadhyay S., Nakamura-Messenger K., Nittler L., Palma R., Pepin R. O., Papanastassiou D. A., Robert F., Schlutter D., Snead C. J., Stadermann F. J., Stroud R., Tsou P., Westphal A., Young E. D., Ziegler K., Zimmermann L. and Zinner E. (2006) Isotopic compositions of cometary matter returned by Stardust. *Science* **314**, 1724–1728.
- McKeegan K. D., Kallio A. P. A., Heber V. S., Jarzebinski G., Mao P. H., Coath C. D., Kunihiro T., Wiens R. C., Nordholt J. E., Moses R. W., Reisenfeld D. B., Jurewicz A. J. G. and Burnett D. S. (2011) The oxygen isotopic composition of the Sun inferred from captured Solar wind. *Science* **332**, 1528–1532.
- Mostefaoui S., Kita N. T., Togashi S., Tachibana S., Nagahara H. and Morishita Y. (2002) The relative formation ages of ferromagnesian chondrules inferred from their initial aluminum-26/aluminum-27 ratios. *Meteorit. Planet. Sci.* **37**, 421–438.
- Nagahara H. (1981) Evidence for secondary origin of chondrules. *Nature* **292**, 135–136.
- Nagahara H. and Ozawa K. (2012) The role of exchange reactions in oxygen isotope fractionation during CAI and chondrule formation. *Meteorit. Planet. Sci.* **47**, 1209–1228.
- Nagahara H., Kita N. T., Ozawa K. and Morishita Y. (2008) Condensation of major elements during chondrule formation and its implication to the origin of chondrules. *Geochim. Cosmochim. Acta* **72**, 1442–1465.
- Nakamura T., Noguchi T., Tsuchiyama A., Ushikubo T., Kita N. T., Valley J. W., Zolensky M. E., Kakazu Y., Sakamoto K., Mashio E., Uesugi K. and Nakano T. (2008) Chondrulelike objects in short-period comet 81P/Wild 2. *Science* **321**, 1664–1667.
- Nakashima D., Ushikubo T., Gowda R. N., Kita N. T., Valley J. W. and Nagao K. (2011) Ion microprobe analyses of oxygen three-isotope ratios of chondrules from the Sayh al Uhaymir 290 CH chondrite using a multiple-hole disk. *Meteorit. Planet. Sci.* **46**, 857–874.
- Nyquist L. E., Kleine T., Shih C. Y. and Reese Y. D. (2009) The distribution of short-lived radioisotopes in the early Solar system and the chronology of asteroid accretion, differentiation, and secondary mineralization. *Geochim. Cosmochim. Acta* **73**, 5115–5136.
- Rambaldi E. R. (1981) Relict grains in chondrules. *Nature* **293**, 558–561.
- Rowe M. W., Clayton R. N. and Mayeda T. K. (1994) Oxygen isotopes in separated components of CI and CM meteorites. *Geochim. Cosmochim. Acta* **58**, 5341–5347.
- Rubin A. E. and Krot A. N. (1996) Multiple heating of chondrules. In *Chondrules and the Protoplanetary Disk* (eds. R. H. Hewins, R. H. Jones and E. R. D. Scott). Cambridge Univ. Press, Cambridge, pp. 173–180.
- Rudraswami N. G., Ushikubo T., Nakashima D. and Kita N. T. (2011) Oxygen isotope systematics in the Allende CV3 chondrite: high precision ion microprobe studies. *Geochim. Cosmochim. Acta* **75**, 7596–7611.
- Ryerson F. J. and McKeegan K. D. (1994) Determination of oxygen self-diffusion in akermanite, anorthite, diopside, and spinel: implications for oxygen isotopic anomalies and the thermal histories of Ca–Al-rich inclusions. *Geochim. Cosmochim. Acta* **58**, 3713–3734.
- Ryerson F. J., Durham W. B., Cherniak D. J. and Lanford W. A. (1989) Oxygen diffusion in olivine: effect of oxygen fugacity and implications for creep. *J. Geophys. Res.* **94**, 4105–4118.
- Sakamoto N., Seto Y., Itoh S., Kuramoto K., Fujino K., Nagashima K., Krot A. N. and Yurimoto H. (2007) Remnants of the early Solar System water enriched in heavy oxygen isotopes. *Science* **317**, 231–233.
- Schrader D. L., Connolly, Jr., H. C., Lauretta D. S., Nagashima K., Huss G. R., Davidson J. and Domanik K. J. (2013) The formation and alteration of the Renazzo-like carbonaceous chondrites II: linking O-isotope composition and oxidation state of chondrule olivine. *Geochim. Cosmochim. Acta*. <http://dx.doi.org/10.1016/j.gca.2012.09.045>.

- Scott E. R. D. and Jones R. H. (1990) Disentangling nebular and asteroidal features of the CO₃ carbonaceous chondrites. *Geochim. Cosmochim. Acta* **54**, 2485–2502.
- Scott E. R. D. and Krot A. N. (2003) Chondrites and their components. In *Meteorites Comets and Planets, vol. 1* (ed. A. M. Davis) (eds. H. D. Holland and K. K. Turekian). Elsevier-Pergamon, Oxford, pp. 143–200.
- Scott E. R. D., Love S. G. and Krot A. N. (1996) Formation of chondrules and chondrites in the protoplanetary nebula. In *Chondrules and the Protoplanetary Disk* (eds. R. H. Hewins, R. H. Jones and E. R. D. Scott). Cambridge Univ. Press, Cambridge, pp. 87–96.
- Shibata Y. (1996) Opaque minerals in Antarctic CO₃ carbonaceous chondrites, Yamato-74135, -790992, -791717, -81020, -81025, -82050 and Allan Hills-77307. In *20th Symp. Antarctic Meteorites*, vol. 9. pp 79–96.
- Thiemens M. H. and Heidenreich J. E. (1983) The mass-independent fractionation of oxygen – a novel isotope effect and its possible cosmochemical implications. *Science* **219**, 1073–1075.
- Tsuchiyama A., Nagahara H. and Kushiro I. (1980) Experimental reproduction of textures of chondrules. *Earth Planet. Sci. Lett.* **48**, 155–165.
- Tsuchiyama A., Nagahara H. and Kushiro I. (1981) Volatilization of sodium from silicate melt spheres and its application to the formation of chondrules. *Geochim. Cosmochim. Acta* **45**, 1357–1367.
- Tsuchiyama A., Osada Y., Nakano T. and Uesugi K. (2004) Experimental reproduction of classic barred olivine chondrules: open-system behavior of chondrule formation. *Geochim. Cosmochim. Acta* **68**, 653–672.
- Ushikubo T., Kimura M., Nakashima D. and Kita N. T. (2010) A combined study of the Al–Mg systematics and O isotope ratios of chondrules from the primitive carbonaceous chondrite Acfer 094. *Lunar Planet. Sci. XLI*. Lunar Planet. Inst., Houston. #1491 (abstr.).
- Ushikubo T., Kimura M., Kita N. T. and Valley J. W. (2012) Primordial oxygen isotope reservoirs of the Solar nebula recorded in chondrules in Acfer 094 carbonaceous chondrites. *Geochim. Cosmochim. Acta* **90**, 242–264.
- Villeneuve J., Chaussidon M. and Libourel G. (2009) Homogenous distribution of ²⁶Al in the Solar System from the Mg isotopic composition of chondrules. *Science* **325**, 985–988.
- Wadhwa M., Bouvier A. and Brennecka A. (2011) Concordant early Solar System timescales from Pb–Pb and extinct chronometers. *Meteorit. Planet. Sci.* **46**, A245 (abstr.).
- Wasson J. T. and Rubin A. E. (2003) Ubiquitous low-FeO relict grains in type II chondrules and limited overgrowths on phenocrysts following the final melting event. *Geochim. Cosmochim. Acta* **67**, 2239–2250.
- Wasson J. T., Krot A. N., Lee M. S. and Rubin A. E. (1995) Compound chondrules. *Geochim. Cosmochim. Acta* **59**, 1847–1869.
- Wasson J. T., Rubin A. E. and Yurimoto H. (2004) Evidence in CO_{3.0} chondrules for a drift in the O isotopic composition of the Solar nebula. *Meteorit. Planet. Sci.* **39**, 1591–1598.
- Yu Y. and Hewins R. H. (1998) Transient heating and chondrule formation: evidence from sodium loss in flash heating simulation experiments. *Geochim. Cosmochim. Acta* **62**, 159–172.
- Yu Y., Hewins R. H., Clayton R. N. and Mayeda T. K. (1995) Experimental study of high temperature oxygen isotope exchange during chondrule formation. *Geochim. Cosmochim. Acta* **59**, 2095–2104.
- Yurimoto H. and Wasson J. T. (2002) Extremely rapid cooling of a carbonaceous-chondrite chondrule containing very ¹⁶O-rich olivine and a ²⁶Mg-excess. *Geochim. Cosmochim. Acta* **66**, 4355–4363.
- Yurimoto H. and Kuramoto K. (2004) Molecular cloud origin for the oxygen isotope heterogeneity in the Solar system. *Science* **305**, 1763–1766.
- Yurimoto H., Ito M. and Nagasawa H. (1998) Oxygen isotope exchange between refractory inclusion in Allende and Solar nebula gas. *Science* **282**, 1874–1877.
- Yurimoto H., Krot A. N., Choi B.-G., Aléon J., Kunihiro T. and Brearley A. J. (2008) Oxygen isotopes of chondritic components. In *Reviews in Mineralogy and Geochemistry*, vol. 68 (ed. G. J. MacPherson). Mineralogical Society of America, Washington, D.C., pp. 141–186.
- Zanda B., Bourrodenise M., Perron C. and Hewins R. H. (1994) Origin and metamorphic redistribution of silicon, chromium, and phosphorus in the metal of chondrites. *Science* **265**, 1846–1849.

Associate editor: Alexander N. Krot